# Wormlike micellar solutions II: comparison between experimental data and scission model predictions

C. J. Pipe [a,*], N. J. Kim [a,b], G. H. McKinley [a], P. A. Vasquez [c], L. P. Cook [c]

[a] *Hatsopoulos Microfluids Laboratory, Department of Mechanical Engineering, Massachusetts Institute of Technology, Cambridge, MA 02139, USA.*

[b] *School of Chemical Engineering, Seoul National University, San 56-1 Shillim-dong, Seoul 151-744, Korea.*

[c] *Department of Mathematical Sciences, University of Delaware, Newark, DE 19716, USA.*

**Abstract**

Although many constitutive models for wormlike micellar solutions have been proposed, few quantitative comparisons have been made with detailed rheological measurements. The majority of comparative studies focus on the linear viscoelastic properties of micellar solutions, which are well described by monoexponential Maxwell-like behavior. In the present work we compare the predictions of a prototypical two-species reptation-reaction model (developed in Part 1, Vasquez et al, 2007) with rheological measurements performed using a concentrated cetyl pyridinium chloride/sodium salicylate (CPyCl/NaSal) solution in a range of steady and transient shear flows. The model captures the continuous rupture and reformation of the

long entangled chains that form a physically-entangled viscoelastic network and the enhanced breakage rates that occur during imposed shearing deformations.

In homogeneous shearing flows the model describes numerous qualitative features of the linear and nonlinear rheology; including a strong strain-dependent damping function during large strains, agreement with the Lodge-Meissner rule at moderately large strains, large rate-dependent first normal stress coefficients in steady shear flow and pronounced stress overshoots during start-up of steady shear. The present model cannot predict the second normal stress difference observed experimentally or the persistent agreement with the Lodge-Meissner rule observed experimentally at very large strains. Homogeneous flow calculations with this simplified two species model cannot capture quantitatively the full range of transient dynamics observed experimentally. More complex time-dependent test protocols, including step-jumps (up and down) in deformation rate and applied stress, are used to reveal the slow temporal dynamics associated with evolution of the shear-banding plateau. Such experiments help to provide insight into additional features (such as diffusion coefficients for stress-microstructure coupling) that are required for fully-quantitative rheological equations of state describing these concentrated wormlike micellar solutions.

## 1 Introduction

Wormlike micelles are high aspect ratio flexible chains of surfactant molecules in solution which self-assemble under an appropriate combination of solvent,

* Corresponding author. Present address: Nestlé Research Center, Vers-chez-les-Blanc, PO Box 44, 1000 Lausanne 26, Switzerland

*Email addresses:* christopherjames.pipe@rdls.nestle.com (C. J. Pipe), nanjido@snu.ac.kr (N. J. Kim), gareth@mit.edu (G. H. McKinley), vasquez@udel.edu (P. A. Vasquez), cook@math.udel.edu (L. P. Cook).

surfactant, and counter-ions. Unlike conventional polymer chains, these wormlike microstructures have the remarkable ability to break and then recombine, hence the name "living polymers" (Anderson *et al.*, 2006*a*; Cates & Fielding, 2006). Understanding the rheology of these solutions is of considerable practical interest due to their wide class of applications, ranging from household and personal care products to oil recovery. Accordingly, these wormlike micellar systems have been well studied both experimentally (Cates & Candau, 1990; Rehage & Hoffmann, 1991; Méndez-Sánchez *et al.*, 2003; Yesilata *et al.*, 2006) and theoretically (Cates, 1987; Granek & Cates, 1992; Olmsted *et al.*, 2000), and a large variety of rheological behaviours has been observed in these solutions depending on surfactant and co-surfactant concentration. Here we focus on systems of semi-dilute entangled wormlike micelles (Berret *et al.*, 1994, 1997; Miller & Rothstein, 2007; Davies *et al.*, 2010) which form highly elastic and heavily shear-thinning solutions but which do not show shear-induced structure formation or shear-thickening at high deformation rates (eg. Boltenhagen *et al.*, 1997; Fischer *et al.*, 2002).

The linear viscoelastic response of these liquids is now well known: for small deformations and low frequencies the response of the micellar network is well described by a Maxwell fluid with a single relaxation time $\lambda$ and an elastic modulus $G_N^0$ (Rehage & Hoffmann, 1991; Kern *et al.*, 1994). However, instead of reaching the asymptotic values of $G' \to G_N^0$ and $G'' \to \omega^{-1}$ for high frequency deformations $\omega \gg \lambda^{-1}$, as would be characteristic of a perfect Maxwellian fluid, both the elastic and loss moduli slowly increase with frequency. This phenomenon is associated with the onset of Rouse modes of relaxation (Turner & Cates, 1991). Further, as the amplitude of deformation imposed on the micellar network increases beyond the linear domain, a strain-

dependent response is observed which may be characterized by a damping function $h(\gamma)$ (Brown *et al.*, 1997; Bautista *et al.*, 1999) so that the shear stress in the system is described as $\tau_{xy} = G(t)h(\gamma)$.

The Maxwell-like description also holds for steady flow experiments at low shear rates where the solutions exhibit a shear-rate-independent viscosity $\eta_0 = G_N^0\lambda$ (Rehage & Hoffmann, 1991). At strain rates above approximately $\lambda^{-1}$ the steady state shear viscosity of the micellar solutions is strongly shear-thinning. Given the right conditions in concentration and temperature this decrease in the viscosity with increasing shear rate approaches an asymptotic slope of $-1$ giving rise to a region in which the shear stress is nearly constant for a wide range of shear rates. This region of the flow curve is commonly referred to as the stress plateau. The stress plateau region is associated with the presence of shear-banded flow (Berret *et al.*, 1994; Schubert *et al.*, 2004) and has been the focus of considerable attention (Grand *et al.*, 1997; Decruppe *et al.*, 2001; López-González *et al.*, 2004; Fielding & Olmsted, 2006). In particular, it has been shown that this shear-banding behavior can be predicted by constitutive equations that result in a non-monotonic viscometric flow curve (Spenley *et al.*, 1993; Porte *et al.*, 1997; Olmsted *et al.*, 2000). Slow transient responses lasting hundreds of relaxation times have also been reported in this plateau region (Grand *et al.*, 1997; Porte *et al.*, 1997) which suggest the possibilities of thixotropy and shear-induced phase transitions (Berret *et al.*, 1994; Schubert *et al.*, 2004) and can lead to chaotic fluctuations in the shear stress (Ganapathy & Sood, 2006; Pimenta & Pashkovski, 2006). Finally, at very high shear rates, the shear plateau ends and the shear stress increases again with further increases in rate; however, this part of the flow curve can be difficult to access experimentally using a standard rheometer due to the onset of more

complex flow instabilities, demixing, and foaming (Berret *et al.*, 1994; Yesilata *et al.*, 2006). These problems can be somewhat mitigated by using microfluidic rheometry which offers the possibility to impose very high deformation rates without the presence of a free surface (Pipe *et al.*, 2008; Nghe *et al.*, 2008).

Recently, a variety of other non-linear flows have been explored to better understand the rheological properties of wormlike micellar solutions, including the start up of steady shear flow (Soltero *et al.*, 1999), large amplitude oscillatory deformations (Méndez-Sánchez *et al.*, 2003), steady flows with superposed oscillations (Anderson *et al.*, 2006*b*) and strong extensional deformations (Rothstein, 2003; Yesilata *et al.*, 2006; Bhardwaj *et al.*, 2007).

### *1.1 Constitutive modeling*

Early rheological data indicated that wormlike micellar solutions resemble a familiar entangled polymeric structure but possess quantitatively different dynamics. These observations inspired the 'reptation-reaction' model of Cates (1987) which coupled the original reptation model for entangled polymer solutions proposed by de Gennes (1971) and by Doi & Edwards (1986) with reaction equations to capture the breaking and reforming of the living polymer chains following a prescribed probability distribution. Cates showed that in the fast breaking limit, in which micellar chains break on a time scale $\lambda_{\rm br}$ which is very short compared to the reptation time $\lambda_{\rm rep}$, a mono-exponential stress relaxation is recovered for small deformations, agreeing well with experimental observations. In addition Cates showed that in that limit, $\lambda_{\rm br} \ll \lambda_{\rm rep}$, the effective elastic relaxation time $\lambda$ of the micellar network is equal to the geometric mean of the breaking and reptation times, $\lambda \approx (\lambda_{\rm br}\lambda_{\rm rep})^{1/2}$.

As we have noted above, further experimental studies revealed transient responses many hundreds of times greater than the elastic relaxation time near the onset of the stress plateau region (Grand *et al.*, 1997; Porte *et al.*, 1997). These long time scales and sigmoidal time signature inspired an analogy between the evolution of the stress-strain rate field in a micellar system and the dynamics observed in thermodynamic phase transitions (Porte *et al.*, 1997). This comparison helps motivate qualitative models that adequately describe the pricipal features of the measured flow curve. However, no complete constitutive theory exists and this analogy lacks the mechanisms to account for linear viscoelastic responses that occur on the effective relaxation time of the network ($t \sim \lambda$) or nonlinear elastic effects such as normal stress differences.

A phenomenological framework for modeling the dynamics of micellar systems in shear flow was proposed by Bautista and coworkers (Bautista *et al.*, 1999; Soltero *et al.*, 1999; Manero *et al.*, 2002). Their approach incorporates a convected Maxwell model coupled with a scalar evolution equation for a parameter characterizing the state of the system's microstructure. They showed that the Fredrickson model (Fredrickson, 1970) for the evolution of the solution fluidity $\phi = \eta^{-1}$ (i.e. the reciprocal of the viscosity) as a function of time and imposed kinematics was able to describe various aspects of micellar solution behaviour. Bautista and coworkers' approach qualitatively captures the non-linear response to step strains and step strain rates and the failure of the Cox-Merz relation that is observed experimentally in these systems. However, the model does not capture the normal stress response measured in wormlike micellar solutions (Anderson *et al.*, 2006*a*). In addition, the flow is assumed to be homogeneous throughout the system, whereas detailed pointwise measurements of the flow show the formation of shear bands of differing shear

rates within the stress plateau region (Britton & Callaghan, 1997; Salmon *et al.*, 2003; Hu & Lips, 2005; Liberatore *et al.*, 2006; Miller & Rothstein, 2007; Davies *et al.*, 2010).

The consequences of spatial variations of the local velocity field on the length scale of a polymer chain and the resulting stress-driven diffusivity of molecules away from local regions of high gradients of velocity and stress were first considered by El-Kareh & Leal (1989), Bhave *et al.* (1991) and Mavrantzas & Beris (1992) within the framework of the kinetic theory for dumbbells - which is most applicable for dilute solutions of flexible polymer chains. Spenley and Cates (Spenley *et al.*, 1993, 1996) extended the original 'reptation-reaction' model of Cates to nonlinear flows and arrived at a Doi-Edwards-like model that focused on reptation of the longest species alone and led to a non-monotonic flow curve which, as mentioned above, can describe shear banding behavior. However only predictions for a 'toy model' were considered in detail and no comparison between theory and experiments was presented.

Olmsted and coworkers (Lu *et al.*, 2000; Olmsted *et al.*, 2000) merged the two concepts above by adapting the nonmonotonic Johnson-Segalman model (Johnson & Segalman, 1977) for polymer solutions to include 'non-local' effects which give rise to diffusive gradients in the stress and become important in rapidly-varying regions such as shear-bands. Calculations show that even in the absence of diffusive effects this model captures many of the features of nonlinear shearing flows of micellar solutions, including sharp spatial variations such as shear-banding and hysteresis in the flow curve during rate sweeps (Lu *et al.*, 2000; Olmsted *et al.*, 2000). More recently it has been demonstrated that it can also predict periodic fluctuations in the structure of the shear bands (Fielding & Olmsted, 2006). Unfortunately this model cannot accu-

rately describe results of step strain shearing flows due to the form of the Gordon–Schowalter derivative. This non-affine convected derivative is directly connected with the nonmonotonic stress variation and enables the prediction of shear-banding; however it cannot readily be connected to microstructural processes such as scission/reforming events.

Cook and coworkers (Cook & Rossi, 2004; Rossi *et al.*, 2006) developed a model that is derived from the kinetic theory of dumbbells to incorporate both non-affine motion and spatial variations in the local number density of the micelles which are modeled as Hookean dumbbells. This model incorporates non-affine motions or 'slippage' into previous dumbbell models (Bhave *et al.*, 1991; Mavrantzas & Beris, 1992) via the Gordon-Schowalter derivative and was studied computationally under steady state shear in plane (Cook & Rossi, 2004) and circular Couette flows (Rossi *et al.*, 2006). However, even though this model included in a self-consistent manner local number density variations, like earlier variants of the Johnson-Segalman model, the model is phenomenological in nature and hence cannot be directly compared to actual physical processes of rupture and reformation in the micellar network.

In the present work we compare, on a quantitative basis, rheological measurements in both linear and nonlinear shear flows with the predictions of a rheological equation of state that describes the coupling in the micellar microstructure, the local fluid kinematics and the resulting macroscopic stress. The constitutive model is described in detail in Part I of this work (Vasquez *et al.*, 2007, or for brevity VCM) and an overview is included here in the appendix. The VCM model was formulated to capture a number of the key physical ideas outlined above; including the presence of an entangled elastic

network, continuous rupture and reformation of chains, and a coupling between the local number density profile of micelles and gradients in the stress and velocity distributions which can lead to evolution in the macroscopic response over long time scales.

The VCM model incorporates earlier constitutive developments as outlined in Table 1. In contrast to earlier constitutive equations, this family of two species models captures individual contributions to the total viscoelastic stress arising from long entangled chains (species 'A') and from a shorter, unentangled 'B' species. The models are self-consistently derived from kinetic network theory and aim to capture the coupling between the local microstructural conformation and the resulting macroscopic stress response (Vasquez *et al.*, 2007; Zhou *et al.*, 2008). Like earlier investigations, these models can be studied in homogeneous (viscometric) flows, in which the kinematics are specified a priori, or in more complex (inhomogeneous) situations in which the local kinematic variations in the flow field (such as the onset of shear-banding transitions) are coupled to the local state of stress in the fluid. If the local number density $n_A$ of the longer chains evolves due to dynamic breaking and reforming events, then the VCM model describes the dynamics and shear-banding observed in concentrated micellar solutions. Large localized stress gradients in the vicinity of the shear-bands also result in 'non-local' effects such as stress-induced diffusion.

If breaking and reforming events are disallowed, then $n_A$ and $n_B$ remain constant; however the VCM model still describes shear-banding transitions, and a plateau in the steady shear flow-curve, as a result of non-affine deformation of the elastic network and disentanglement of the longer 'A' chains. In this *non-breaking limit* the two-mode VCM model involves fewer material constants

and evolution equations (Larson, 1988). If the short chains comprising the 'B' species have a vanishingly small relaxation time $\lambda_B \rightarrow 0$ then their rheological response is essentially Newtonian; in this limit the model reduces to the partially-extending convected (PEC) equation proposed by Larson (Larson, 1984) as a differential analog of the Doi-Edwards reptation model for entangled melts. In the non-breaking limit, the corresponding two-mode model is denoted 'PEC+M' because the 'A' species evolve according to the PEC equation of state, and the shorter 'B' species are governed by an upper-convected Maxwell model.

Before considering the full complexity of inhomogeneous flows and shear-banding, we first explore the capabilities and limitations of viscometric flow calculations with the VCM model. To this end, in the present work we consider how well the two mode VCM model can describe measurements of the steady and transient rheology of a well-characterized wormlike micelle system. We present detailed rheological measurements of a CPyCl/NaSal micellar solution in unidirectional shear flows. The experiments explore shear deformations for a wide range of amplitudes and frequencies. In particular we examine the onset and development of the non-linear response at large deformation amplitudes and large deformation rates. As outlined above, we compare experimental results with predictions from the VCM model for homogeneous flow in order to better understand the strengths and limitations of the model for describing wormlike micellar flow dynamics. In turn the behavior of the model is used to infer information on the microstructural processes leading to the onset of shear-banded flow.

This work is organized as follows: in Section 2 we describe our experimental procedures and the preparation of the test fluid. Results are presented and

discussed in Section 3; including small amplitude oscillatory shear measurements (3.1), decay of the shear stress and normal stress after a step strain (3.2), the steady state response in shear flow (3.3), transient response after the start up and cessation of steady shear flow (3.4), slow transients in steady shearing flow (3.5), transient evolution of the strain rate after the start up of steady stress-controlled flow (3.6) and, finally, probes of the transient approach to the steady flow curve following step changes in the deformation rate (3.7). Conclusions are summarized in Section 4 with respect to the non-linear shear rheology of the micellar system, the transition to non-linear flow and the performance of the homogeneous VCM model in capturing the dynamics of the wormlike micellar system.

## 2 Experimental procedure

In this work we investigate surfactant solutions of cetylpyridinium chloride (CPyCl, $m_0 = 340$ g/mol) and sodium salicylate (NaSal, $m_0 = 160.1$ g/mol) dissolved in brine. Such systems have been studied extensively in the past, for example by Berret and coworkers (Berret *et al.*, 1993, 1994), Rothstein and coworkers (Rothstein, 2003; Miller & Rothstein, 2007) and elsewhere (López-González *et al.*, 2004; Hu & Lips, 2005). For a fixed 2:1 ratio of surfactant to counterion, the concentration regimes for CPyCl/NaSal were mapped out in Berret *et al.* (1993) and Berret *et al.* (1994). It was found that the cross-over from a dilute to semi-dilute solution occurs at a surfactant concentration of 0.4 wt% (12.5 mM) and the transition from a semi-dilute to a concentrated solution occurs at a surfactant concentration of 6 wt% (190 mM). In the present work we focus on a solution of 100 mM/50 mM (3.2 wt%/0.76 wt%)

CPyCl/NaSal in a 100 mM (0.56 wt%) NaCl solution, which lies towards the upper end of the semi-dilute regime. This system has been studied previously (Miller & Rothstein, 2007; Bhardwaj *et al.*, 2007; Davies *et al.*, 2010) and is far away from phase boundaries for the solution at rest.

Rheological measurements were performed using an ARES controlled rate rheometer (Rheometric Scientific) and an AR-G2 controlled stress rheometer (TA Instruments). Cone and plate geometries were used with a radius of 30 mm and an angle of 2.0° on the AR-G2 rheometer and a radius 50 mm with an angle of 2.3° on the ARES. Unless stated otherwise, all of the experiments reported were carried out at 22°C and using a solvent trap to minimize evaporation of the sample. Due to the high elasticity of the micellar solutions, great care was taken when loading the samples in the rheometer: a small pre-shear was applied during loading to ensure that the sample was distributed evenly throughout the gap after which the sample was allowed to sit and rest for 2 minutes ($\gtrsim$ 100 viscoelastic relaxation times) to allow any residual stresses to decay. Also, between experimental runs the sample was left to sit and rest for 2 minutes to ensure that residual viscoelastic stresses from previous measurements had decayed. The first normal stress difference was measured using the normal force transducers of the ARES and the AR-G2 rheometers. Estimates of the second normal stress difference were determined from the radial pressure distribution measured using a RheoSense pressure transducer array (RheoSense Inc., San Ramon, CA) mounted on the upper fixture of the ARES (Baek & Magda, 2003).

## 3 Results and discussion of results

### *3.1 Small Amplitude Oscillatory Shear (SAOS) Flow*

In Figure .1(a) we present the linear viscoelastic (LVE) response of the 100 mM CPyCl/NaSal solutions to small amplitude oscillations ($\gamma_0 \leq 0.3$) at temperatures $T$ over the range 20°C–50°C. The results are presented in terms of reduced storage and loss moduli $G'_{\rm r}+{\rm i}G''_{\rm r} = G^*_{\rm r}(\omega_{\rm r}, T_{\rm ref}) = (T_{\rm ref}/T)G^*_T(\omega, T)$ and the reduced angular frequency $\omega_{\rm r} = a_T\omega_T$ where the reference temperature is $T_{\rm ref} = 22$°C. The viscoelastic stress response superposes well across the range of temperatures measured and the shift factor $a_T$ (Figure .1(b)) is well described by a classical Arrhenius dependence:

$$a_T = \exp\left[\frac{\Delta\tilde{H}}{R}\left(\frac{1}{T} - \frac{1}{T_{\rm ref}}\right)\right], \tag{1}$$

where $\Delta\tilde{H}$ is the activation energy for flow and $R$ is the molar gas constant. For our micellar solution $\Delta\tilde{H}/R = 1.8 \times 10^4$ K. It should be noted that such a high activation energy indicates that the physical properties of the micellar solution can vary greatly with small temperature fluctuations.

For frequencies $\omega \leq 5$ rad s$^{-1}$ the data at 22°C show good agreement with a single mode Maxwell fluid with a relaxation time $\lambda = 0.64$ s, an elastic modulus of $G^0_N = 22.6$ Pa, and a zero-shear-rate viscosity $\eta_0 = \lambda G^0_N = 14.5$ Pa s. These values are in good agreement with previously reported data for similar concentration CPyCl/NaSal solutions at similar temperatures (Berret *et al.*, 1993). The best fit value of $G^0_N = 22.6$ Pa was estimated using a Cole-Cole representation of the LVE data as shown in Figure .2; in this form, a Maxwellian fluid exhibiting mono-exponential relaxation describes a semi-circle with a di-

ameter equal to $G_N^0$. Only data up to the maximum measured value of $G''$ (i.e. data at low frequencies, $\lambda\omega < 1$) were used for fitting purposes, as this is the range of frequencies over which single exponential relaxation behaviour is expected. In this region the breaking time $\lambda_{\rm br}$ of the micelles is very small compared to the time-scale of the applied deformation and the location and orientation of individual micellar segments within the network are quickly 'forgotten' resulting in a purely exponential relaxation. As discussed by Turner & Cates (1991), the data represented on a Cole-Cole plot can also be used to help to understand the response of the micellar network to high frequency deformations. As the time scale of the applied deformation approaches that of $\lambda_{\rm br}$, deviation from a single mode Maxwell model is observed and the stress relaxation occurs increasingly through reptation processes, indicated by a line of slope -1 on linear axes. Further increases in frequency lead to the onset of breathing modes of stress relation and eventually Rouse modes. In the Cole-Cole representation the latter modes are signified by a change in sign of the gradient. Hence, we estimate the Rouse time $\lambda_{\rm R}$ of this micellar network from the reciprocal of the frequency at which the gradient becomes positive at high frequencies in the Cole-Cole diagram, $\lambda_{\rm R} \approx 1/(40\ {\rm rad\,s^{-1}}) = 0.025$ s.

Predictions of length and time scales of the micellar network can be obtained by combining results from the reptation-reaction model of Cates with those from classical reptation theory. The ratio of the entanglement length $l_{\rm e}$ to the average length of a micellar chain $\bar{L}$ is given by (Granek & Cates, 1992):

$$\frac{G''_{\rm min}}{G_N^0} \sim \frac{l_{\rm e}}{\bar{L}}, \tag{2}$$

where $G''_{\rm min}$ is the value of $G''$ at the local minimum observed at intermediate frequencies $\lambda^{-1} < \omega < \lambda_{\rm R}^{-1}$. From the reptation model (Doi & Edwards, 1986)

we can find $l_e$ from the relationship:

$$l_e \sim \xi^{5/3} b^{-2/3}, \tag{3}$$

where the correlation length is $\xi = (k_B T / G_N^0)^{1/3} = 55$ nm and the persistence length is $b \sim 15$ nm (Berret *et al.*, 1993). Combining equation (2) and (3) we find that the average micellar length is $\bar{L} \sim 1.2$ $\mu$m and the distance between entanglements is $l_e \sim 0.13$ $\mu$m.

The apparent relaxation time $\lambda$ is related to the breaking time $\lambda_{br}$ and the reptation time $\lambda_{rep}$ by $\lambda = (\lambda_{br}\lambda_{rep})^{1/2}$ (Cates, 1987). We use the quantity $\bar{\zeta} = \lambda_{br}/\lambda$, as defined in Turner & Cates (1991), and the ratio of $G_N^0/G_\infty$ to calculate the breaking time. For this we use Figure 2 in Turner & Cates (1991) in which the diameter of the fitted semicircle to the Cole-Cole plot (DFS) is related to the parameter $\bar{\zeta}$. For our system $G_N^0 = 22.6$ Pa and the elastic modulus for very quick displacements is $G_\infty = 24.0$ Pa. Note that in a multispecies model the plateau modulus $G_N^0$ and $G_\infty$ are not identical because the latter quantity also captures elastic contributions of the shorter chains and $G_\infty$ is estimated using the results from step strain experiments presented in section 3.2. Now, taking DFS = 0.94 as the ordinate value in the Figure 2 of Turner & Cates (1991), we find $\bar{\zeta} \approx 0.15$. Finally, taking the value $\lambda = 0.64$ s from SAOS experiments, we find $\lambda_{br} \approx 0.10$ s and $\lambda_{rep} \approx 4.10$ s.

In Figure .1(a) we have also plotted the prediction of the VCM model for the loss and storage moduli. In the linear viscoelastic regime, this model behaves as the superposition of two Maxwell modes with relaxation times $\lambda$ and $\lambda_B$ respectively. The latter (shorter) time scale is the relaxation time of the shorter species and is responsible for the upturn in $G'$ and $G''$ predicted at higher frequencies. This upturn in the loss modulus is a direct consequence

of the breakage of chains at high frequencies and the dynamics of the system happening in time scales comparable to Rouse relaxation times, i.e., relaxation of shorter species. Note that this upturn in the loss modulus at high frequencies is usually captured in one-species models by the addition of an unphysically large solvent viscosity. As discussed in Vasquez *et al.* (2007), to determine the value of the model parameters we use regression to both SAOS and step strain data. From those fittings we find $\lambda = 0.63$s and $\lambda_B = 0.0011$s. Predictions from the model agree well with experimental data at low and high frequencies, however the quality of the fitting decreases at intermediate frequencies. This lack of agreement is a consequence of 'lumping' together all long species into a single elastically-active network segment (species A) and all short species into species B. From the fittings, after we determine $\mu = 10$, we find that the longest relaxation time of the elastic strands is $\lambda_A = 6.3$s. As expected, this is of the same order as the reptation time in the original Cates model. In the VCM model the effective relaxation time is reduced from the relaxation time of the long strands (even in the absence of any flow) due to the additional processes of worm scissions such that:

$$\frac{1}{\lambda} = \frac{1}{\lambda_A} + c'_{A\,\mathrm{eq}}, \tag{4a}$$

or equivalently:

$$\lambda = \frac{\lambda_A}{1 + c'_{A\,\mathrm{eq}}\lambda_A}, \tag{4b}$$

where the breaking rate at equilibrium is determined from the fitting to be $c'_{A\,\mathrm{eq}} = 1.4286\mathrm{s}^{-1}$.

*3.2 Step strain*

In Figure .3 (a) we show the time evolution of the elastic modulus $G(t) = \tau_{xy}(t)/\gamma_0$ after a step strain $\gamma_0$. For small strains the stress decays exponentially and fitting a Maxwell relaxation model to the data, $G(t) = G_\infty \exp(-t/\lambda)$ gives $\lambda = 0.63$ s and $G_\infty = 24$ Pa. These values are in excellent agreement with those found in SAOS; $G_\infty = 24$ Pa found in step strain is consistent with the SAOS data at $\omega \approx 20$ rad s$^{-1}$ where $G'$ is slightly larger than the stress plateau value $G_N^0 = 22.6$ Pa. At long times after the applied strain, a single exponential stress relaxation with a constant relaxation time is seen for all applied strains, suggesting that the stress relaxation process at long times is independent of $\gamma_0$. This is clearly illustrated in Figure .3 (b) where the measured modulus is scaled to ensure superposition at $t = \lambda$. For long times $t > \lambda$ the experimental data show that stresses relax in a similar manner regardless of the applied strain. At short times $t \ll \lambda$, however, the stress relaxation is strongly dependent on the magnitude of the applied strain. As noted in Section 3.1, at high frequencies (short times) both Rouse and reptation modes of stress relaxation are observed. After step strains of $\gamma_0 > 1$ , the residual memory of the initial configuration of the network is significant and these relaxation mechanisms dominate at short times. The initial configuration of the micellar network is 'forgotten' after $t \gtrsim \lambda_{\rm br} = 0.1$ s due to the continual breaking and reforming of the network segments and the stresses subsequently relax exponentially. The initial decrease in modulus at large applied strains is commonly referred to as *strain-softening*.

Calculations of the VCM model under step strain were performed imposing a

strain history given by:

$$\gamma(t) = \gamma_0 \left(1 - (1 + bt)\, e^{-bt}\right), \tag{5}$$

where the parameter $b$ is obtained through fitting to the experimental motor response of the controlled strain rheometer. The effects of varying $b$ were explored in Zhou *et al.* (2008). For all the calculations in this paper $b = 62\,\mathrm{s}^{-1}$ which approximately captures the response of the ARES rheometer. The parameter $b$ controls the duration of the ramp of the applied strain, so that in Figure .3(a) the time $t_{\max}$ at which the local maximum in the shear stress is observed corresponds approximately to the maximum in the prediction from the model, $t_{\max} = 1/b$.

The amount of strain softening is a function of the relaxation mechanisms of the different elastic strands within the network. To see this we first consider the non-breaking limit ($c'_{A\,\mathrm{eq}} = 0$). In the framework of polymer reptation theory, at long times, relaxation occurs mainly through reptation. In contrast, at much shorter times retraction of the chains within their tubes is the dominant mechanism. The degree of retraction depends on how rapidly the deformation is applied, i.e. on the strength of the external flow. As a result partial retraction determines the amount of strain softening (Larson *et al.*, 1999). In wormlike micellar systems, in addition to reptation and Rouse relaxation, relaxation occurs due to the continuous rupture of the wormlike micelles. For such systems, strain softening is a function of the Rouse-like relaxation of shorter chains, reptation of the longer chains, and the chain breakage rate. In the VCM model the rupture processes are captured by the enhanced breaking rate:

$$c_A = c_{A\,\mathrm{eq}} + \frac{1}{3}\xi\mu \left(\dot{\boldsymbol{\gamma}} : \frac{\mathbf{A}}{n_A}\right). \tag{6}$$

Regression of the model predictions to step strain experiments thus allows us to determine the value of the non-linear breakage parameter $\xi$. Numerical calculations show that the best description of the data is obtained for $\xi = 0.5$.

Inspection of Figure .3(a) shows that the VCM model provides a good qualitative description of the short time dynamics and can quantitatively describe the long time single exponential character of the stress decay. The model underpredicts the extent of strain-softening observed at very large strains $\gamma_0 > 6$. The lack of qualitative agreement at short times is to be expected because of the 'lumping' of the shorter chain contributions into a single species 'B'.

The shift factor necessary to collapse the elastic modulus measurements in Figure .3 (b) at long times $t \geq \lambda$ is called the damping function $h(\gamma_0)$ (here calculated to ensure superposition at $t = \lambda$). The variation in the damping $h(\gamma_0)$ as a function of the applied strain is shown in Figure .4. The damping function for the CPyCl/NaSal solution is fitted with the approximate form predicted by the single-mode PEC tube model assuming an infinitely fast step strain (Larson, 1988),

$$h(\gamma_0) = \frac{1}{1 + \xi' \gamma_0^2/3}, \tag{7}$$

and a value of $\xi' = 0.52$ closely predicts the observed strain softening. Over the range of experimental data the agreement is striking, although reasonable: strain-softening in the micellar network is principally due to chain disentanglement at $t < 0.2$ s and processes other than breaking of the micelles dominate. These features can be well captured in models such as the PEC model describing non-affine deformation of a polymeric network. However, although the values of the damping function are well predicted by the PEC model, this model fails to capture the full behavior of the relaxation modulus in time,

i.e. Figure .3 (a). The mechanisms involved in the strain softening process for wormlike micellar solutions are similar to those observed in polymeric systems, but the exact response of the full breaking dynamics in which a single long chain can reptate or break with equal probability along its length cannot be captured by a single species model.

We note that for applied strains $\gamma_0 < 1$ and $\gamma_0 > 5$ the behaviour observed for the CPyCl/NaSal solutions is similar to that described by Brown *et al.* (1997) for a cetyltrimethylammonium bromide(CTAB) system; however, at intermediate strains $1 < \gamma_0 < 5$ the CPyCl/NaSal solutions do not show the strain-stiffening reported in Brown *et al.* (1997). Inhomogeneous flow calculations with the PEC model (Zhou *et al.*, 2008) predict spatial shear banding will occur over a range of intermediate strains. Thus predictions of the full inhomogeneous VCM model in large amplitude step strains will be different than the viscometric predictions.

In Figure .5 (a) we present measurements of the stress ratio $N_1(t)/\tau_{xy}(t)$ (i.e the ratio of the first normal stress difference to the shear stress) after a step strain $\gamma_0$ is applied. For rapid stretching of an ideal Gaussian network the Lodge-Meissner rule gives $N_1(t)/\tau_{xy}(t) = \gamma_0$. For step strains $\gamma_0 < 8$, the ratio $N_1/\tau_{xy}$ measured experimentally follows the imposed motor response function given by equation 5 and then remains constant after $O(0.1$ s). For larger step strains the response shows a maximum at $t \sim 0.1$ s, after which the relative decrease in $N_1$ compared with $\tau_{xy}$ indicates that the first normal stress difference strain-softens more strongly than the shear stress. At very large strains $\gamma_0 > 10$, $N_1/\tau_{xy}$ shows a weak overshoot and becomes independent of $\gamma_0$. This can be seen clearly in Figure .5 (b) in which the value of the stress ratio $N_1/\tau_{xy}$ at $t^* = 0.2$ s is plotted as a function of $\gamma_0$. The time $t^*$ is

selected to be longer than the response time of the motor but shorter than the effective relaxation time $b^{-1} < t^* < \lambda$. The Lodge-Meissner prediction for affine network deformations, $N_1/\tau_{xy} = \gamma_0$, holds for strains up to $\gamma_0 = 8$, which is clearly well into the non-linear deformation régime. As discussed in Larson (1988) this is commonly observed for concentrated polymer solutions and indicates the strongly elastic component of the response to step strains.

The predictions of the VCM model are shown in in Figure .5 by the solid red lines. We see that the values of the stress ratio at large strains calculated from the *viscometric* VCM model are significantly smaller than those measured experimentally. As discussed by Zhou *et al.* (2008), considering a homogenous flow *a priori* results in a decrease of the magnitude of predicted first normal stress difference, and this can be clearly seen in Figure 11(b) of Zhou *et al.* (2008). Calculations for smaller deformations below the anticipated onset of banding $\gamma_0 \leq 2$ are consistent with experimental measures and satisfy the Lodge-Meissner relationship. Further investigations for inhomogeneous flows are required to reveal if the discrepancies between model and observation at very large strains are reduced when the kinematic conditions are no longer assumed to be viscometric (homogenous).

### *3.3 Steady state response in shear flow*

The evolution in the steady state shear stress $\tau_{xy}$ of the micellar solution due to an imposed shear rate $\dot{\gamma}_0$ is shown in Figure .6 (a). These experiments were performed using the ARES controlled strain instrument and (as will be discussed in greater detail in § 3.5) steady state flow was achieved for all measurements after 120 s. At low shear rates, the measured stress increases

linearly with applied shear rate implying a constant viscosity $\eta_0 = \tau_{xy}/\dot{\gamma}_0$, indicated by the solid blue line in fig. .6 (a) with a value consistent with the limiting value obtained from SAOS data at low frequencies $\omega \ll 1/\lambda$. At shear rates above $\dot{\gamma}_0 \sim 1/\lambda$ the onset of shear-thinning is observed and for shear rates $3 \leq \dot{\gamma}_0 \leq 100$ s$^{-1}$, strong apparent shear-thinning is present, giving rise to a 'plateau' in the measured steady state flow curve. The value of $\tau_{xy}$ at which this plateau occurs is approximately $0.8G_N^0$ which is similar to the value reported elsewhere in the literature for this system at similar concentrations (Berret *et al.*, 1994). Although not presented here, independent verification has shown that the empirical Cox–Merz rule overpredicts the measured shear stress $\tau_{xy}(\dot{\gamma})$ in the plateau region, in close agreement with previous work (Berret *et al.*, 1994). As we have noted, the plateau region is associated with the development of an inhomogeneous shear-banded flow (Britton & Callaghan, 1999; Manneville *et al.*, 2005; Miller & Rothstein, 2007). Thus homogeneous calculations with the VCM model should not be expected to quantitatively capture this plateau.

Although shear-induced demixing transitions are not anticipated in this system (Berret *et al.*, 1994), at very high shear rates $\dot{\gamma}_0 \gtrsim 150$ s$^{-1}$, large normal stresses cause the sample to foam at the air-sample interface and the behaviour of this micellar system at very high rates is largely unexplored. Recently, measurements from a narrow gap parallel plates geometry and straight microchannels have been used to investigate the steady state flow curve of this system and a CTAB in sodium nitrate ($NaNO_3$) solution up to shear rates of $\dot{\gamma}_0 \sim 10^4$ s$^{-1}$ Pipe *et al.* (2008); Nghe *et al.* (2008). The resulting flow curves indicate that the shear stress continues to increase weakly after the plateau region although more detailed investigations are needed to understand the

behaviour at shear rates $\dot{\gamma}_0 > 1000\ \mathrm{s}^{-1}$.

The steady state first normal stress difference $N_1$ as a function of applied shear rate $\dot{\gamma}_0$ measured using the ARES normal stress transducer is shown in Figure .6 (b). At low rates, $N_1$ increases quadratically with $\dot{\gamma}_0$ to within experimental error, indicating a constant normal stress coefficient $\Psi_1$. Simple fluid theory predicts that at low deformation rates $\dot{\gamma}_0 \leq \lambda^{-1}$ the storage modulus $G'$ is related to $N_1$ in the following way:

$$\lim_{\dot{\gamma}_0 \to 0} \frac{N_1(\dot{\gamma})}{\dot{\gamma}_0^2} = \lim_{\omega \to 0} \frac{2G'(\omega)}{\omega^2}. \tag{8}$$

Within experimental uncertainty this is valid for $\dot{\gamma}_0 \lesssim 1\mathrm{s}^{-1}$ (fig .6 (b)).

As $\dot{\gamma}_0$ increases above 1 $\mathrm{s}^{-1}$, $N_1$ continues to increase but less rapidly than quadratically. It should be noted that the degree of shear-thinning of $\Psi_1$ is not as dramatic as observed for the shear viscosity and no plateau in the normal stress flow curve is seen. This observation provides a useful discrimination between many empirical constitutive equations proposed for wormlike micellar solutions.

It is now well understood that a non-monotonic viscometric flow curve is a sufficient condition for a constitutive equation to be able to model shear banding behavior, for recent reviews see Dhont & Briels (2008) and Olmsted (2008). In contrast to existing models (with the exception of that proposed by Spenley and Cates, Spenley *et al.* (1993)), the non-monotonic behavior in the VCM model arises exclusively from the breaking and reforming of strands, and hence it can directly connect the dynamics of the shear-banding process with the interaction of the different species present in these wormlike micellar systems. The forms of the non-monotonic viscometric flow curve predicted by

the VCM model for $\tau_{xy}$ and $N_1$ are shown in Figure .6 (with all parameters determined from small amplitude and step strain data). Note that, as pointed out before, assuming viscometric flow results in an under-prediction of the stresses for shear rates $\dot{\gamma}_0 > 1\text{s}^{-1}$. For an inhomogeneous (non-viscometric) flow, we would expect a closer agreement between the model and experiments with $N_1$ growing monotonically with shear stress, the gradient of the curve depending on the breaking and reformation of the different species. Representative inhomogeneous calculations in the non-breaking limit for the simpler PIC+M model also show a monotomic variation in $N_1(\dot{\gamma})$ (Zhou *et al.*, 2008).

We now investigate the behaviour of the second normal stress difference $N_2$ in a cone-and-plate configuration using a microfabricated pressure sensor array (Baek & Magda, 2003). The static pressure at the plate $\Pi_{\theta\theta}(r)$ is monitored as a function of shear rate at eight radial locations across the diameter. Viscometric flow calculations with the CEF model show that the total static excess pressure should decrease logarithmically with radius in a cone and plate fixture (Bird *et al.*, 1987):

$$\Pi_{\theta\theta} - p_{\text{a}} = -(N_1 + 2N_2)\log\left(\frac{r}{R}\right) - N_2, \tag{9}$$

Where $r$ is the radial coordinate and $R$ is the radius of the cone and plate geometry. Extrapolating this expression radially to $r = R$ to provide an estimate of the thrust at that location $[\Pi_{\theta\theta}]_R$ allows the second normal stress coefficient $\Psi_2$ to be calculated:

$$\Psi_2 = \frac{p_{\text{a}} - [\Pi_{\theta\theta}]_R}{\dot{\gamma}^2}, \tag{10}$$

where $p_{\text{a}}$ is the atmospheric pressure. Typical measurements of $\Pi_{\theta\theta}(r) - p_{\text{a}}$ are shown in Figure .7 (a) for $10 \leq \dot{\gamma}_0 \leq 150$ s$^{-1}$ and fits used to calculate

$[\Pi_{\theta\theta}]_R - p_a$ in Equation (10) are shown as dotted lines. A positive intercept with the line $r = R$ gives a negative value of $\Psi_2$ and the error in finding the intercept is about $\pm 20\%$. For shear rates up to $\dot{\gamma}_0 = 50$ s$^{-1}$, the data are well described by Equation 9 and the local thrust varies logarithmically across the stationary lower fixture of the rheometer. However, at higher shear rates, the radial dependence becomes more complex. As shown in Britton & Callaghan (1997), shear-banding of a micellar solution in a cone-plate fixture is a function of radial location as well as shear rate and this effect may be expected to result in a non-logarithmic radial static pressure profile (Lee *et al.*, 2002). Extrapolation of Equation 9 to $r = R$ is thus of limited utility beyond $\dot{\gamma}_0 \approx 50$ s$^{-1}$.

The first normal stress coefficient $\Psi_1$ can also be calculated from these measurements using Eq. 9 and the values found from the pressure sensor array agree with the values measured using the normal force transducer of the ARES to within the error of the technique for rates $\dot{\gamma}_0 \leq 50$ s$^{-1}$. For these experiments, we were unable to control the temperature of the CPyCl/NaSal sample because the experimental configuration precluded the use of a temperature control system. Measurements were performed at $T = 21.3 \pm 0.3$°C and within a single experimental run, the temperature varied by less than 0.1°C. Therefore although there will be some uncertainty introduced by changes in temperature between data points, it should not be significant.

The ratio of the normal stress coefficients $-\Psi_2/\Psi_1$ is shown in Figure .7 (b). At low shear rates the relative error is large because values of the thrust are small. However, $-\Psi_2/\Psi_1$ appears to be larger than the value that is predicted by the Doi-Edwards model ($-\Psi_2/\Psi_1$=0.28) for a reptating polymer network and we find $-\Psi_2/\Psi_1 \approx 0.4$ up to shear rates $\dot{\gamma} = 50$ s$^{-1}$. This implies that

the zero shear second normal stress coefficient $\Psi_{20} \approx 4$ Pa s$^2$. The large error bars highlight that values of $\Psi_2$ presented here are susceptible to error, because small variations in the slope fitted to $\Pi_{\theta\theta}(r)$ can potentially lead to significantly different values of $\Psi_1$ and $\Psi_2$. We emphasize that all data used to calculate the second normal stress coefficient $\Psi_2(\dot{\gamma})$ presented here are well into the steady state shear-banding regime (i.e. $\lambda\dot{\gamma}_0 > 1$); the velocity field in a cone and plate apparatus may thus be radially inhomogeneous (Britton & Callaghan, 1999) rendering Eqn. (10) and subsequent calculations of $\Psi_2$ inaccurate.

The nonlinear Giesekus model, which describes anisotropic drag on network segments (through a single nonlinear coefficient $\alpha$), does predict non-zero second normal stress differences and the ratio $-\Psi_2/\Psi_1 \to \alpha/2$ in the limit $\dot{\gamma} \to 0$. This suggest a value of $\alpha \approx 0.8$ which is consistent with previous fits of the Giesekus model to measurements of the shear viscosity $\eta(\dot{\gamma})$ and normal stress $N_1(\dot{\gamma})$ in wormlike micellar solutions (Fischer & Rehage, 1995; Yesilata *et al.*, 2006; Helgeson *et al.*, 2009).

Experiments by Lee *et al.* (2002) show that for a shear-thickening and *dilute* CTAB wormlike micellar solution the normal stress coefficient ratio is $-\Psi_2/\Psi_1 = 0.16$, which Ð in contrast to the CPyCl/NaSal system used in the current study Ð is smaller than the prediction from the Doi-Edwards model (although the authors suggested that the the results showed reasonable agreement to within experimental error). It was also shown that the measured value of $-\Psi_2/\Psi_1$ was constant over the shear rate range for which a logarithmic profile could reasonably be assumed. Furthermore, the emergence of a non-logarithmic radial static pressure profile, was found to occur well after the transition to inhomogeneous flow. These observations agree qualitatively with the results reported here. It should be noted that because of the assumed

affine deformation of the individual Hookean elastic strands, the VCM model predicts a second normal stress coefficient $\Psi_2 = 0$ Pa s$^2$ at all deformation rates.

### *3.4 Start up and cessation of steady shear flow*

We continue to examine the response of the micellar network to non-linear deformations by investigating the transient stress response during the start up of steady shear flow. For times $t < 0$ s, $\dot{\gamma}_0 = 0$ s$^{-1}$ and the fluid is in equilibrium and at $t = 0$ s a step increase in the shear rate $\dot{\gamma}_0$ is applied. We show experimental measurements of the evolution in shear stress $\tau_{xy}$ and normal stress difference $N_1$ following the start up of steady shear flow in Figures .8 (a) and (b), respectively. It should be noted that the stresses are represented on a logarithmic scale because of the wide dynamic range in the data . Figure .8 (a) shows that for small shear rates the shear stress response $\tau_{xy}(t)$ of the network is well described by that of a Maxwell fluid with $\lambda = 0.63$ s and $G_N^0 = 22.6$ Pa. This description holds for $\dot{\gamma}_0 \lesssim 0.8$ s$^{-1}$, corresponding to $\lambda\dot{\gamma}_0 \lesssim 0.5$. However, as the applied shear rate is increased two principal deviations from Maxwellian behaviour are observed. First, the onset of non-linear viscoelasticity manifests itself with the presence of a stress overshoot at short times ($t < \lambda$), which is followed by subsequent stress under- and overshoots for sufficiently large steps in shear rate, similar to those reported by Ganapathy & Sood (2008) for a cetyltrimethylammonium tosylate (CTAT) micellar system. Second, as is well known for concentrated entangled solutions of wormlike micelles, the steady-state viscosity $\eta(\dot{\gamma})$ is strongly shear-thinning and the steady state value of $\tau_{xy}$ at long times does not increase linearly with

$\dot{\gamma}_0$; at large rates $\dot{\gamma}_0 > 3\ \mathrm{s}^{-1}$ the presence of a stress plateau in the shear stress attained at long times can be seen.

Figure .8 (b) shows that after applying a step increase in shear rate from rest the first normal stress difference $N_1(t)$ is also well represented by a Maxwell fluid for small deformation rates $\dot{\gamma}_0 \lesssim 0.8\mathrm{s}^{-1}$. For larger values of shear rate, $N_1$ also exhibits an overshoot at short times $t < 3\lambda$ as well as a shear-thinning first normal stress coefficient $\Psi_1(\dot{\gamma}_0)$. However, as previously noted, there is no evidence of a plateau in the first normal stress difference at high shear rates.

The homogeneous VCM model is able to capture quantitatively the transient response of both the shear stress and first normal stresses at moderate shear rates $\lambda\dot{\gamma}_0 = 0.64\ \mathrm{s} \times 5\ \mathrm{s}^{-1} = 3.2$, close to the beginning of the shear stress plateau. However, at the highest shear rates, the predictions of the homogeneous calculations differ significantly from the measured data. Qualitative features such as the rapid rise in the stress at very short times followed by a sharp overshoot and more rapid approach to steady state are captured. However, the quantitative magnitudes are substantially underpredicted. This is not unexpected when the predicted steady viscometric repsonse shown in Figure .6 is reconsidered. If a homogeneous flow is assumed *a priori* then the VCM model predicts a non-monotonic response for shear rates $\dot{\gamma}_0 > 5\ \mathrm{s}^{-1}$. In addition, the stress overshoots predicted by the VCM model are observed for shear rates above $\dot{\gamma}_0 \sim 5\ \mathrm{s}^{-1}$, which is the same point at which the constitutive prediction for the steady state flow curve starts to decrease.

In addition to the startup of steady shear flow we also examined the rheological response upon cessation of steady shear flow: for $t < 0$ s, $\dot{\gamma} = \dot{\gamma}_0$ and the flow is at steady state, then at $t = 0$ s, the applied deformation is abruptly ceased.

In Figure .9 we see that after cessation of steady flow the shear stress $\tau_{xy}$ decays in a mono-exponential manner for $\dot{\gamma}_0 \lesssim 5$ s$^{-1}$ and the behavior shows good agreement with the Maxwell model. For consistency, we choose to use the values of $\lambda$ and $G_N^0$ calculated independently in the SAOS experiments; however, we note that slightly improved agreement at very low stresses can be obtained using a relaxation time approximately 10% larger. At high shear rates corresponding to the shear-banding régime ($30 \leq \dot{\gamma}_0 \leq 150$ s$^{-1}$), cessation of steady shear flow shows that faster modes of stress relaxation dominate the short time response at $t < 0.2$ s, while at longer times a mono-exponential relaxation is observed. This more rapid rate of stress relaxation is observed and is indicative of a change in the elastic network structure at large deformations. This can be well described in an empirical manner, as shown by the solid black line in Figure .9, by a 2 mode relaxation process:

$$\tau_{xy} \approx Ae^{-t/\lambda_1} + Be^{-t/\lambda_2},$$

with $A = 4.7$ Pa, $B = 17.4$ Pa and $\lambda_1 = 0.64$ s, $\lambda_2 = 0.062$ s for $\dot{\gamma}_0 = 150$ s$^{-1}$. The shorter time constant is close to the value for the breaking time of a micelle $\lambda_{\text{br}} \approx 0.10$ s calculated in § 3.1. This two mode picture is consistent with the initial configuration of the micellar network controlling the stress decay at large deformation rates and short times until this is 'forgotten' due to local breaking/reformation events and the network reverts towards its equilibrium configuration.

### *3.5 Slow transients in start up of steady shear flow*

There has been considerable discussion of slow transient shear stresses in controlled rate flows of wormlike micellar systems and how they can best be de-

scribed (Grand *et al.*, 1997; Porte *et al.*, 1997; Hu & Lips, 2005). These slow approaches to steady-state flow lasting hundreds of viscoelastic relaxation times are observed over a narrow range of stresses (here 19–22 Pa, see Figures .11 & .12) near the onset of inhomogeneous flow and have been described variously as resulting from a mechanical flow instability (Spenley *et al.*, 1996), concentration fluctuations (Schmitt *et al.*, 1995) or a flow-induced phase transition (Porte *et al.*, 1997); although the description offered by Hu & Lips (2005) is more complex. Figures .10 (a) and (b) show the long time stress response to the step strain rate experiments described in § 3.4 using an ARES controlled rate (CR) rheometer and an AR-G2 controlled rate (CS) rheometer, both operating in controlled rate mode. Long transients are indeed present for the CPyCl/NaSal micellar system studied here, with a slow approach to steady state $\tau_{xy}$ occurring over times $O(100\lambda)$. The measurements were performed using similar geometries with the CS and CR instruments, a 50 mm, 2.4° cone and plate fixture with the ARES and 60 mm, 2° cone and plate fixture with the AR-G2, hence it is reasonable to expect similar shear stress responses in the two devices, even in transient flows. Indeed the shear stress signatures are qualitatively similar, both showing long times to reach equilibrium for step shear rates near the onset of the shear banded flow ($\dot{\gamma}_0 = 3$ s$^{-1}$) and stress undershoots for higher step rates ($\dot{\gamma}_0 = 10$ s$^{-1}$). However, even though the steady-state values of $\tau_{xy}$ agree to within 1%, the time needed to reach steady state with the CS instrument is an order of magnitude greater than with the CR device. The CS device achieves a specified deformation rate by controlling the stress acting on the rotating fixture and using a proportional-integral-differential (PID) type control loop to measure and adjust the applied rate of rotation. By contrast, in the controlled rate device, a constant rotation rate is achieved in less than 40 ms. For wormlike micellar solutions in which there are

large transient stresses at short times, followed by a shear stress plateau that leads to pronounced sensitivity to small changes in the applied stress, it is not surprising that a PID feedback algorithm may not perform as effectively in achieving a specified rate of shearing as it does for less non-linear materials.

### *3.6 Start up of flow with a steady applied stress*

After examining the slow stress transients associated with the development of shear-bands in controlled shear rate experiments, the question arises of how the rate of deformation evolves to steady-state during start up of controlled stress flow. Figure .11 shows that at stresses below the onset of the steady-state shear stress plateau ($22 \lesssim \tau_{xy,\ \mathrm{plateau}} \lesssim 23$ Pa), the measured shear rate reaches its steady-state value within a few viscoelastic relaxation times. However, as the applied stress reaches the stress plateau value, slow transients in the measured shear rate with time constants $O(1000\lambda)$ are observed. This is illustrated in Figure .12 which shows the equilibration time required to reach 99% of the final shear rate $t_\mathrm{e}$ as a function of the constant applied stress $\tau_{xy\ 0}$. At low deformation rates (Wi $< 1$), the fluid exhibits a Maxwellian response and the flow quickly reaches steady-state with little fluctuation in the measured rate of shearing. At stresses corresponding to the steady-state stress plateau, very large times $t_\mathrm{e} \gtrsim 1000\lambda$ are necessary to attain the final state, analogous to the long transients observed in shear rate controlled flow. Indeed for the measurements $20.5 \leq \tau_{xy\ 0} \leq 21.5$ no steady state shear rate was achieved within the duration of the experiment (300 s).

At higher imposed stresses the system evolves more rapidly to the higher shear rate branch of the flow curve, although long timescales $\sim 10 - 100\lambda$ are

still required. Again this highlights the slow evolution of shear-banded flow towards a steady state. At high values of the imposed shear stress $\tau_{xy\ 0} >$ 24 Pa pronounced fluctuations are seen in the instantaneous shear rate $\dot{\gamma}(t)$. Unsteady flow in the high shear branch of the flow curve is consistent with results for concentrated wormlike micellar systems reported elsewhere (Nghe *et al.*, 2008).

The trends observed here agree well with those observed by Hu & Lips (2005) in a cylindrical couette geometry. They described two processes in the evolution of the velocity profile: 'shear tilting' in which the shear rate varies continuously across the gap, and shear-banding consisting of a constant rate region connected to a region with a continuously varying shear rate. These two distinct behaviors may account for the two different rate responses observed here; with 'shear tilting' corresponding to the slow increase in rate and shear-banding to the more rapid evolution of $\dot{\gamma}$. The results in Figures .11 & .12 can also be interpreted in terms of nucleation and growth of a local shear-induced phase transition (Porte *et al.*, 1997) at a critical stress $\tau_{xy,\ \mathrm{crit}} \approx$ 21–22 Pa.

### *3.7 Transient flow curve*

Finally, we present data on the transient approach to the steady flow curve (Figure .13 (a)) measured using a CR rheometer. The steady-state flow curve (indicated by the solid line in Figure .13 (a)) may be considered an attractor for this non-linear rheological system. The basin of attraction for this steady state can be explored by observing the transient response in the shear stress to step *increases* in $\dot{\gamma}_0$ from rest (Figure .13 (b)) as well as the transient response to step *decreases* in the imposed shear rate from a large value of 150 $\mathrm{s}^{-1}$, cor-

responding to the right hand branch of the flow curve (Figure .13 (c)). Within the language of nucleation and growth theories, these 'jump' experiments may be considered as analogous to 'undercooled' or 'superheated' thermal states of the material. By plotting the maximum/minimum stress over-/undershoots in response to steps in shear rate (hollow symbols), an envelope containing the range of accessible shear stresses attainable in the system can be mapped out.

The hollow circles in Figure .13 (a) show the maximum shear stress measured during step increases in deformation rate as exemplified by Figure .13 (b). The magnitude of this stress-overshoot increases approximately linearly with deformation rate and the stress then relaxes towards an apparent steady state over a time constant consistent with the effective relaxation time of the network $\lambda$. However, as we have seen in Figure .10, additional slow transients are present at long times associated with stress-induced diffusion of the banded structures.

The corresponding 'step-down' experiments are shown by the hollow triangles in Figure .13 (a) and (c). When the deformation rate is decreased from a value of 150 $s^{-1}$ (corresponding to the upper limit of the stress-induced plateau) down to a lower value, a pronounced antithixotropic-like response is observed. The stress initially drops substantially before recovering to a value consistent with the steady state flow curve. This complex behaviour is due to the transient response of the microstructure and rearrangement of the shear-bands as they adapt to the lower value of the externally-imposed shear rate.

## 4 Conclusions

We have presented a comprehensive comparison between the viscometric flow predictions of the VCM network scission model described in Vasquez *et al.* (2007) and experimental measurements of the steady and transient rheology of a concentrated wormlike micellar system. A brief overview of how the calculations from the model compare to the experimental measurements of the CPyCl/NaSal system is provided in Table 2. The two mode VCM model accurately captures the linear response of the CPyCl/NaSal solution in small amplitude oscillatory shear and small amplitude step strain experiments, as well as the initial non-linear response in homogeneous flows. The single effective relaxation time $\lambda$ observed experimentally corresponds to the reptation time of the long 'A' chains, appropriately reduced due to the effects of chain scission.

The sensitivity of the micellar network to changes in temperature is probed experimentally using small amplitude oscillatory shear measurements for temperatures 18–50°C. A large Arrhenius activation energy $\Delta H = 1.47{\times}10^5$ J/mol is measured, which for a 3°C increase in temperature, corresponds to a 50% decrease in viscometric properties such as viscosity and relaxation time.

In step strain experiments for strains $\gamma_0 > 6$, the measured damping function $h(\gamma_0)$ is over-predicted by the VCM model using the parameter set determined independently from oscillatory measurements. Further refinement of this two mode model to better capture the scission/recombination processes (e.g. allowing the recombination rate $c_{Beq}$ to vary with flow conditions or the presence of a broader spectrum of species) remains the subject of future study.

Experimental measurements of the first normal stress difference after a step strain show that the Lodge–Meissner rule $N_1(t)/\tau_{xy}(t)$ is obeyed by this CPyCl/NaSal solution up to large strains $\gamma_0 \approx 8$, well into the strain softening régime. This is consistent with the picture that for step strains $\gamma_0 < 8$ the micellar network exhibits elastic rubber-like behavior. While the homogeneous flow calculations with the VCM model deviate from the Lodge-Meissner rule for $\gamma_0 > 2$, inhomogeneous flow calculations predict a higher first normal stress difference at large strains and may describe the experimentally-observed response more closely (Zhou *et al.*, 2008).

For steady shearing flow, experimental measurements show a Newtonian viscosity $\eta_0$ at low shear rates $\dot{\gamma}_0 < \lambda^{-1}$ followed by a shear stress plateau occurring at $\tau_{xy} \approx 0.8G_N^0$ for shear rates $\dot{\gamma}_0 > \lambda^{-1}$. This strongly shear-thinning region is associated with the development of shear bands and is consistent with previous results reported for this system (Berret *et al.*, 1994) as well as local velocimetric measurements (Miller & Rothstein, 2007). The homogeneous calculations with the constitutive model predict a non-monotonic flow curve at shear rates $\dot{\gamma}_0 \gtrsim \lambda^{-1}$. The critical conditions for onset of the stress plateau for the VCM model are controlled by the magnitude of the single non-linear model parameter $\xi$. By contrast, in simpler non-linear 'toy models' this value is fixed as a function of viscoelastic properties (Spenley *et al.*, 1996). In the present study, the value of $\xi$ is selected to agree with step strain measurements and then held fixed. This is found to accurately predict the range of shear rates for onset of the stress plateau in steady shear flow, indicating that the model is self-consistent. Accordingly, inhomogeneous calculations for a limiting case of the VCM model were considered in Zhou *et al.* (2008) and a representative calculation with the value of $\xi$ deduced from step strain measurements is pre-

sented in figure 14. This more accurate description of the local kinematics gives rise to a plateau in the flow curve in good agreement with the experimental data. Thus there is a reasonable expectation that considering inhomogeneous velocity fields will lead to improved agreement with experimental results in the stress plateau region.

The first normal stress coefficient measured in steady flow is constant at low shear rates $\dot{\gamma} < \lambda^{-1}$, and both the model and the measurements satisfy the asymptotic limit $\Psi_1(\dot{\gamma}) = 2G'(\omega)/\omega^2$, consistent with a single mode Maxwell fluid. However, while the first normal stress difference flow curve shows considerable shear-thinning of $\Psi_1$ for $\dot{\gamma} > \lambda^{-1}$, no plateau value is observed in the shear banding region. We have also been able to measure the second normal stress difference as a function of the imposed deformation rate for the first time in a shear-thinning micellar fluid: we find that for shear rates up to 50 $s^{-1}$(well into the inhomogeneous banded flow region) the stress ratio $-\Psi_2/\Psi_1 \approx 0.4$. At high shear rates $\dot{\gamma} > 50$ $s^{-1}$, the experimentally measured radial pressure profile no longer varies logarithmically, suggesting the onset of strongly inhomogeneous flow at high shear rates $\dot{\gamma} \sim 100$ $s^{-1}$.

The VCM model is capable of predicting a non-zero first normal stress difference in steady shearing flow, in contrast to certain phenomenonological models (e.g. Bautista *et al.*, 1999), and accurately represents the experimental data prior to the onset of shear banding. Although the homogeneous flow calculations are not expected to reliably describe an inhomgeneous flow, it should be noted that our calculations for inhomogeneous shearing flows also show a marked plateau in the first normal stress coefficient at the inner wall coinciding with the shear stress plateau (Zhou *et al.*, 2008). The VCM model does not predict a 2nd normal stress difference because of the scalar isotropic form

of the nonlinear network rupture term $c_A$. Providing an accurate description of the first and second normal stress differences in inhomogeneous shear flow remains an open challenge for models of wormlike micellar networks.

The slow shear stress transients $\tau_{xy}(t)$ after the start up of steady shearing flow with shear rate $\dot{\gamma}_0$ are explored using both controlled rate and controlled stress rheometers. Both devices show that long transients $O(100\lambda)$ are present near the onset of shear banding. In contrast to previous work (Grand *et al.*, 1997), we observe that the measured response is strongly dependent on whether the rheometer imposes a true controlled rate flow or whether the rate control is only imposed using a feedback routine, with the latter approach giving rise to transient timescales an order of magnitude longer. Considering the highly nonlinear transient response of the fluid, it is not surprising that a PID feedback algorithm may encounter difficulties imposing ideal controlled rate conditions in a constant stress rheometer.

Finally, we have investigated the evolution in the instantaneous shear rate $\dot{\gamma}(t)$ for an imposed constant shear stress $\tau_{xy\ 0}$. As in the corresponding measurements of the stress response after the start up of steady shear flow, we see that imposing stresses near the value of the stress plateau (associated with the onset of shear banded flow) leads to slow transients on time scales of $O(1000\lambda)$.

In summary we have shown that global (i.e. spatially integrated) rheometric measurements at constant stress or deformation rate can certainly offer a useful tool for investigating the transient evolution of shear banding flows. However, there is plenty of scope to investigate local measures of the conformation, concentration and velocity profiles to provide a deeper understanding of the constitutive response of the micellar network. For nonlinear viscoelastic

fluids such as wormlike micellar solutions that exhibit complex deformation-dependent microstructures, quantitatively describing transient responses to non-linear deformations remains a challenge for experimentalists, theorists and numerical modeling alike.

## Appendix: An overview of the VCM Model

The details of the VCM family of models developed in Vasquez *et al.* (2007) are briefly summarized here. In the remainder of the text we focus on a quantitative comparison of the model and measurements in a range of steady and transient shear flows. In the VCM model the entangled wormlike micellar fluid is reduced to a network consisting of two elastically-active species, labeled 'A' and 'B'. Each species is modeled as a Hookean elastic segment of length L and L/2 respectively. The 'A' species continuously breaks and the 'B' species continuously reforms so that $A \rightleftarrows 2B$. This two species model incorporates breakage and reforming dynamics in a discrete version of Cates' 'living polymer' model (Cates, 1987, 1990). The evolution equations for the number density ($n_{\mathrm{A}}$, $n_{\mathrm{B}}$) and stress ($\mathbf{A}$, $\mathbf{B}$) associated with each species are derived systematically from the number density equations formulated in configuration space. The resultant nonlinear number density and constitutive equations (in dimensionless variables) are:

$$\mu \frac{Dn_{\mathrm{A}}}{Dt} - 2\delta_{\mathrm{A}}\nabla^2 n_{\mathrm{A}} + \delta_{\mathrm{A}}\nabla\nabla : \mathbf{A} = \frac{1}{2}c_{\mathrm{B}}n_{\mathrm{B}}^2 - c_{\mathrm{A}}n_{\mathrm{A}}, \tag{.1a}$$

$$\mu \frac{Dn_{\mathrm{B}}}{Dt} - 2\delta_{\mathrm{B}}\nabla^2 n_{\mathrm{B}} + 2\delta_{\mathrm{B}}\nabla\nabla : \mathbf{B} = -c_{\mathrm{B}}n_{\mathrm{B}}^2 + 2c_{\mathrm{A}}n_{\mathrm{A}}, \tag{.1b}$$

$$\mu\mathbf{A}_{(1)} + \mathbf{A} - n_{\mathrm{A}}\mathbf{I} - \delta_{\mathrm{A}}\nabla^2\mathbf{A} = c_{\mathrm{B}}n_{\mathrm{B}}\mathbf{B} - c_{\mathrm{A}}\mathbf{A}, \tag{.2a}$$

$$\epsilon\mu\mathbf{B}_{(1)} + \mathbf{B} - \frac{n_{\mathrm{B}}}{2}\mathbf{I} - \epsilon\delta_{\mathrm{B}}\nabla^2\mathbf{B} = -2\epsilon c_{\mathrm{B}}n_{\mathrm{B}}\mathbf{B} + 2\epsilon c_{\mathrm{A}}\mathbf{A}, \tag{.2b}$$

where $c_A$ and $c_B$ are the breaking and reformation rate of species A and B respectively. In equations 1–2, $c_B = c_{Beq}$ is constant and $c_A = c_{Aeq} - \frac{\xi}{3}\dot{\gamma} : \mathbf{A}$ where $c_{Aeq}$ is constant and $\xi$ is a parameter controlling stress-induced micelle breakage. Thus the breakage rate depends on the scalar product of the local stress and shear rate which provides a quantitative measure of the local rate of energy dissipation. In viscometric flow predictions these constitutive equations are solved assuming the kinematics are known, specifically that the shear rate is spatially uniform and is the average shear rate imposed across the gap (homogeneous flow) with no slip at the walls.

The following non-dimensionalization of the governing equations is employed:

$$\mathbf{r} = \frac{\mathbf{r}'}{d}, \quad t = \frac{t'}{\lambda}, \quad \mathbf{v} = \mathbf{v}'\frac{\lambda}{d}, \quad \{\mathbf{QQ}\}_\alpha = \frac{H_A\{\mathbf{Q}'\mathbf{Q}'\}_\alpha}{n_A'^0 kT}, \quad n_\alpha = \frac{n'_\alpha}{n_A'^0},$$

where $\alpha = A, B$; $\mathbf{r}'$ is the radial coordinate; $\mathbf{v}'$ is the local velocity; $d$ is a macroscopic characteristic length; $\mathbf{Q}'$ is the end to end vector of an individual chain; $\sqrt{n_A'^0 kT/H_A}$ is a microscopic characteristic length scale; $H_A$ is the spring constant of species A; $k$ is the Boltzmann constant; $T$ is the temperature; and $n_A'^0$ is the dimensional value of the equilibrium number density of the long species $A$. With this scaling the non-dimensional parameters of the model are given by:

$$\epsilon = \frac{\lambda_B}{\lambda_A}, \qquad \mu = \frac{\lambda_A}{\lambda} = 1 + c_{A\,\mathrm{eq}}, \qquad \delta_A = \frac{De}{Pe}, \qquad \delta_B = \frac{1}{3\epsilon}\frac{De}{Pe},$$

with the Deborah number $De = \lambda v'/d$ and the Peclet number $Pe = v'd/D_A$ where $D_A$ is the diffusivity of species A. The parameter $\mu^{-1}$ represents the reduction of the overall effective relaxation time of the network $\lambda$ from the

(longest) relaxation time of the elastic chains $\lambda_A$ as a result of the additional chain rupture mechanism.

Ultimately for full inhomogeneous flow predictions these equations must be coupled to the equations of conservation of mass and of momentum:

$$\boldsymbol{\nabla} \cdot \mathbf{v} = 0, \tag{.3a}$$

$$E^{-1} \frac{D\mathbf{v}}{Dt} = \boldsymbol{\nabla} \cdot \boldsymbol{\Pi}, \tag{.3b}$$

where $\boldsymbol{\Pi} = \boldsymbol{A} + 2\boldsymbol{B}$ is the total stress in the system and $E = \lambda\eta_0/(\rho d^2)$ is the elasticity number. It is this coupling that generates the spatial inhomogeneities and shear banding. The formulation of the model and the analysis for viscometric flows (in which the kinematics are specified) is developed in Part 1 of this work (Vasquez *et al.*, 2007).

In the case of viscometric flow, the derivatives of the stress are zero, so that there are five parameters in the model which physically represent equilibrium breakage and reforming times, the relaxation time of each species in the absence of breakage, and the single nonlinear parameter ($\xi$) controlling the stress/shear rate induced breakage. Strategies for determining these five parameters in the model ($\epsilon, \mu, c_{Aeq}, c_{Beq}, \xi$) are outlined in the previous paper (Vasquez *et al.*, 2007). The loss of homogeneous flow and formation of shear-bands leads to coupling between spatial inhomogeneities and diffusion of micellar species. The width of the shear bands and the dynamics of evolution are controlled by the diffusivities $\delta_A$ and $\delta_B$. These aspects are considered by Zhou *et al.* (2008) where the full inhomogeneous flow of a simpler model, the PEC model, a limiting case of the VCM model is examined in time-dependent shear-rate-controlled experiments and in step strain experiments.

## References


Anderson, V. J., Pearson, J. R. A. & Boek, E. S. 2006*a* *Rheology Reviews 2006*, chap. The rheology of worm-like micellar fluids, pp. 217–253. British Society of Rheology.

Anderson, V. J., Pearson, J. R. A. & Sherwood, J. D. 2006*b* Oscillation superimposed on steady shearing: Measurements and predictions for wormlike micellar solutions. *J. Rheol.* **50** (5), 771–796.

Baek, S. G. & Magda, J. J. 2003 Monolithic rheometer plate fabricated using silicon micromachining technology and containing miniature pressure sensors for n1 and n2 measurements. *J. Rheol.* **47** (5), 1249–1260.

Bautista, F., de Santos, J. M., Puig, J. E. & Manero, O. 1999 Understanding thixotropic and antithixotropic behavior of viscoelastic micellar solutions and liquid crystalline dispersions. I. the model. *J. Non-Newtonian Fluid Mech.* **80**, 93–113.

Berret, J.-F., Appell, J. & Porte, G. 1993 Linear rheology of entangled wormlike micelles. *Langmuir* **9**, 2851–2854.

Berret, J.-F., Porte, G. & Decruppe, J.-P. 1997 Inhomogeneous shear flows of wormlike micelles: a master dynamic phase diagram. *Phys. Rev. E* **55** (2), 1668–1676.

Berret, J.-F., Roux, D. C. & Porte, G. 1994 Isotropic-to-nematic transition in wormlike micelles under shear. *J. Phys. II France* **4**, 1261–1279.

Bhardwaj, A., Miller, E. & Rothstein, J. P. 2007 Filament stretching and capillary breakup extensional rheometry measurements of viscoelastic wormlike micelle solutionsmicelle solutions. *J. Rheol.* **51** (4), 693–719.

Bhave, A. V., Armstrong, R. C. & Brown, R. A. 1991 Kinetic-theory and rheology of dilute, nonhomogeneous polymer-solutions. *J. Chem. Phys.*

**95** (4), 2988–3000.

Bird, R. B., Armstrong, R. C. & Hassager, O. 1987 *Dynamics of Polymeric Liquids, vol 1*, 2nd edn. John Wiley and Sons.

Boltenhagen, P., Hu, Y., Matthys, E. F. & Pine, D. J. 1997 Observation of bulk phase separation and coexistence in a sheared micellar solution. *Physical Review Letters* **79** (12).

Britton, M. M. & Callaghan, P. T. 1997 Two-phase shear band structures at uniform stress. *Phys. Rev. Lett.* **78** (26), 4930–4933.

Britton, M. M. & Callaghan, P. T. 1999 Shear banding instability in wormlike micellar solutions. *Eur. Phys. J. B* **7**, 237–249.

Brown, E. F., Burghardt, W. R. & Venerus, D. C. 1997 Tests of the Lodge-Meissner relation in anomalous nonlinear step strain of an entangled wormlike micelle solution. *Langmuir* **13**, 3902–3904.

Cates, M. E. 1987 Reptation of living polymers: dynamics of entangled polymers in the presence of reversible chain-scission reactions. *Macromolecules* **20**, 2289–2296.

Cates, M. E. 1990 Nonlinear viscoelasticity of wormlike micelles (and other reversibly breakable polymers). *J. Chem. Phys.* **94** (1), 371–375.

Cates, M. E. & Candau, S. J. 1990 Statics and dynamics of worm-like surfactant micelles. *J. Phys.: Condens. Matter* **2**, 6869–6892.

Cates, M. E. & Fielding, S. M. 2006 Rheology of giant micelles. *Advances in Physics* **55** (7-8), 799–879.

Cook, L. P. & Rossi, L. F. 2004 Slippage and migration in models of dilute wormlike micellar solutions and polymeric fluids. *Journal of Non-Newtonian Fluid Mechanics* **116** (2-3), 347 – 369.

Davies, C. J., Sederman, A. J., Pipe, C. J., McKinley, G. H., Gladden, L. F. & Johns, M. L. 2010 Rapid measurement of transient velocity

evolution using gervais. *Journal of Magnetic Resonance* **202** (1), 93–101.

Decruppe, J. P., Lerouge, S. & Berret, J. F. 2001 Insight in shear banding under transient flow. *Phys. Rev. E* **63**, 022501.

Dhont, J. K. G. & Briels, W. J. 2008 Gradient and vorticity banding. *Rheologica Acta* **47** (3), 257–281.

Doi, M. & Edwards, S. F. 1986 *The theory of polymer dynamics*. Oxford University Press.

El-Kareh, A. W. & Leal, L. G. 1989 Existence of solutions for all Deborah numbers for a non-Newtonian model modified to include diffusion. *J. Non-Newtonian Fluid Mech.* **33** (3), 257–287.

Fielding, S. M. & Olmsted, P. D. 2006 Nonlinear dynamics of an interface between shear bands. *Phys. Rev. Lett.* **96**, 104502.

Fischer, P. & Rehage, H. 1995 Quantitative description of the non-linear flow-properties of viscoelastic surfactant solutions. *Progr Col Poly Sci* **98**, 94–98.

Fischer, P., Wheeler, E. K. & Fuller, G. G. 2002 Shear-banding structure orientated in the vorticity direction observed for equimolar micellar solution. *Rheologica Acta* **41** (1), 35–44.

Fredrickson, A. G. 1970 A model for the thixotropy of suspensions. *AIChE J.* **16** (3), 436–441.

Ganapathy, R. & Sood, A. K. 2006 Intermittency route to rheochaos in wormlike micelles with flow-concentration coupling. *Phys. Rev. Lett.* **96** (108301).

Ganapathy, R. & Sood, A. K. 2008 Nonlinear flow of wormlike micellar gels: Regular and chaotic time-dependence of stress, normal force and nematic ordering. *Journal of Non-Newtonian Fluid Mechanics* **149** (1-3), 78–86.

de Gennes, P. G. 1971 Reptation of a polymer chain in the presence of fixed obstacles. *J. Chem. Phys.* **55** (2), 572–579.

Grand, C., Arrault, J. & Cates, M. E. 1997 Slow transients and metastability in wormlike micelle rheology. *J. Phys. II France* **7**, 1071–1086.

Granek, R. & Cates, M. E. 1992 Stress relaxation in living polymers: results from a Poisson renewal model. *J. Chem. Phys.* **96** (6), 4758–4767.

Helgeson, M. E., Vasquez, P. A., Kaler, E. W. & Wagner, N. J. 2009 Rheology and spatially resolved structure of cetyltrimethylammonium bromide wormlike micelles through the shear banding transition. *J. Rheol.* **53**, 727–756.

Hu, Y. T. & Lips, A. 2005 Kinetics and mechanism of shear banding in entangled micellar solutions. *J. Rheol.* **49** (5), 1101–1027.

Johnson, M. & Segalman, D. 1977 A model for viscoelastic fluid behavior which allows non-affine deformation. *J. Non-Newtonian Fluid Mech.* **2**, 255–270.

Kern, F., Lequeux, F., Zana, R. & Candau, S. J. 1994 Dynamical properties of salt-free viscoelastic micellar solutions. *Langmuir* **10**, 1714–1723.

Larson, R. G. 1984 A constitutive equation for polymer melts based on partially extending strand convection. *J. Rheol.* **28** (5), 545–571.

Larson, R. G. 1988 *Constitutive equations for polymer melts and solutions*. Buttersworth.

Larson, R. G., Hu, H., Smith, D. E. & Chu, S. 1999 Brownian dynamics simulations of a dna molecule in an extensional flow field. *Journal of Rheology* **43** (2), 267–304.

Lee, J.-Y., Magda, J. J., Hu, H. & Larson, R. G. 2002 Cone angle effects, radial pressure profile, and second normal stress difference for shear-

thickening wormlike micelles. *Journal of Rheology* **46** (1), 195–208.

Liberatore, M. W., Nettesheim, F., Wagner, N. J. & Porcar, L. 2006 Spatially resolved small-angle neutron scattering in the 1-2 plane: A study of shear-induced phase-separating wormlike micelles. *Physical Review E (Statistical, Nonlinear, and Soft Matter Physics)* **73** (2), 020504.

López-González, M. R., Holmes, W. M., Callaghan, P. T. & Photinos, P. J. 2004 Shear banding fluctuations and nematic order in wormlike micelles. *Phys. Rev. Lett.* **93**, 268302.

Lu, C. Y. D., Olmsted, P. D. & Ball, R. C. 2000 Effects of nonlocal stress on the determination of shear banding flow. *Phys. Rev. Lett.* **84** (4), 642–645.

Manero, O., Bautista, F., Soltero, J. F. A. & Puig, J. E. 2002 Dynamics of worm-like micelles: the Cox–Merz rule. *J. Non-Newtonian Fluid Mech.* **106** (1), 1–15.

Manneville, S., Bécu, L., Grondin, P. & Colin, A. 2005 High-frequency ultrasonic imaging: A spatio-temporal high-frequency ultrasonic imaging: A spatio-temporal approach of rheology. *Colliods and Surfaces A: Physiochem. Eng. ASPECTS* **270-271**, 194–204.

Mavrantzas, V. G. & Beris, A. N. 1992 Modeling of the rheology and flow-induced concentration changes in polymer solutions. *Phys. Rev. Lett.* **69** (2), 273–276.

Méndez-Sánchez, A. F., López-González, M. R., Rolón-Garrido, V. H., Pérez-González, J. & de Vargas, L. 2003 Instabilities of micellar systems under homogeneous and non-homogeneous flow condtitions. *Rheol. Acta* **42**, 56–63.

Miller, E. & Rothstein, J. P. 2007 Transient evolution of shear banding in wormlike micelle solutions. *J. Non-Newtonian Fluid Mech.* **143** ((1)),

22–37.

Nghe, P., Degre, G., Tabeling, P. & Ajdari, A. 2008 High shear rheology of shear banding fluids in microchannels. *Applied Physics Letters* **93** (20), 204102.

Olmsted, P. D. 2008 Perspectives on shear banding in complex fluids. *RHEOLOGICA ACTA* **47** (3), 283–300.

Olmsted, P. D., Radulescu, O. & Lu, C. Y. D. 2000 Johnson-Segalman model with a diffusion term in cylindrical Couette flow. *J. Rheol.* **44** (2), 257–275.

Pimenta, P. & Pashkovski, E. E. 2006 Rheology of viscoelastic mixed surfactant solutions: Effect of scission on nonlinear flow and rheochaos. *Langmuir* **22** (9), 3980–3987.

Pipe, C. J., Majmudar, T. J. & McKinley, G. H. 2008 High shear rate viscometry. *Rheologica Acta* **47** (5), 621–642.

Porte, G., Berret, J.-F. & Harden, J. L. 1997 Inhomogeneous flows of complex fluids: mechanical instability versus non-equilibrium phase transition. *J. Phys. II France* **7**, 459–472.

Rehage, H. & Hoffmann, H. 1991 Viscoelastic surfactant solutions: model systems for rheological research. *Molecular Physics* **74** (5), 933–973.

Rossi, L. F., McKinley, G. H. & Cook, L. P. 2006 Slippage and migration in Taylor-Couette flow of a model for dilute wormlike micellar solutions. *J. Non-Newtonian Fluid Mech.* **136** (2-3), 79–92.

Rothstein, J. P. 2003 Transient extensional rheology of wormlike micelle solutions. *J. Rheol.* **47** (5), 1227–1247.

Salmon, J.-B., Colin, A. & Manneville, S. 2003 Velocity profiles in shear-banding wormlike micelles. *Phys. Rev. Lett.* **90** (22), 228303(4).

Schmitt, V., Maques, C. M. & Lequeux, F. 1995 Shear induced phase

separation of complex fluids: the role of flow-concentration coupling. *Phys. Rev. E* **52** (4), 4009–4015.

Schubert, B. A., Wagner, N. J., Kaler, E. W. & Raghavan, S. R. 2004 Shear-induced phase separation in solutions of wormlike micelles. *Langmuir* **20** (9), 3564–3573.

Soltero, J. F. A., Bautista, F., Puig, J. E. & Manero, O. 1999 Rheology of cetyltrimethylammonium *p*-toluenesulfate-water system. 3. nonlinear viscoelasticity. *Langmuir* **15**, 1604–1612.

Spenley, N. A., Cates, M. E. & McLeish, T. C. B. 1993 Nonlinear rheology of wormlike micelles. *Phys. Rev. Lett.* **71** (6), 939–942.

Spenley, N. A., Yuan, X. F. & Cates, M. E. 1996 Nonmonotonic constitutive laws and the formation of shear-banded flows. *J. Phys. II France* **6** (4), 551–571.

Turner, M. S. & Cates, M. E. 1991 Linear viscoelasticity of living polymers: a quantitative probe of chemical relaxation times. *Langmuir* **7**, 1590–1594.

Vasquez, Paula A., McKinley, Gareth H. & Pamela Cook, L. 2007 A network scission model for wormlike micellar solutions: I. model formulation and viscometric flow predictions. *Journal of Non-Newtonian Fluid Mechanics* **144** (2-3), 122–139.

Yesilata, B., Clasen, C. & McKinley, G. H. 2006 Nonlinear shear and extensional flow dynamics of wormlike suractant solutions. *J. Non-Newtonian Fluid Mech.* **133**, 73–90.

Zhou, L., Vasquez, P. A., Cook, L. P. & McKinley, G. H. 2008 Modeling the inhomogeneous response and formation of shear bands in steady and transient flows of entangled liquids. *Journal of Rheology* **52** (2), 591–623.

| **Model** | Varying $n$ | Kinematics studied | Stress-driven diffusion | Inertia | Reference |
|---|---|---|---|---|---|
| **Single species** | | | | | |
| Maxwell | - | IH | ✓ | - | El-Kareh & Leal (1989) |
| Maxwell | ✓ | V | ✓ | - | Bhave *et al.* (1991); Mavrantzas & Beris (1992) |
| Johnson-Segalman (JS) | - | IH | - | - | Johnson & Segalman (1977) |
| Spenley & Cates | - | V | - | - | Spenley *et al.* (1993, 1996) |
| JS-Olmsted | - | IH | ✓ | - | Lu *et al.* (2000); Olmsted *et al.* (2000) |
| Geisekus with diffusion | - | IH | ✓ | - | Helgeson *et al.* (2009) |
| JS-slippage | ✓ | IH | ✓ | - | Rossi *et al.* (2006) |
| Partially extending and convecting (PEC) strand | - | V | - | - | Larson (1984) |
| **Two species** | | | | | |
| VCM (Viscometric) | ✓ | V | - | - | Vasquez *et al.* (2007) |
| PEC and PEC+M | - | IH | ✓ | - | Zhou *et al.* (2008) |
| VCM | ✓ | IH | ✓ | ✓ | In preparation |

Table .1. Overview of approaches to modeling the coupled microstructural and macrorheological response of complex fluids such as wormlike micellar solutions. Key: V = viscometric flows (specified kinematics) only; IH = inhomogeneous kinematics; 'varying n' indicates that the local number density of elastically-active species is allowed to vary as a result of 'non-local' effects such as gradients in the stress; the column 'stress-driven diffusion' indicates that the model incorporates self-consistent constitutive terms for the coupled local evolution in stress gradients and number density of species.

| **Flow investigated** | **Comparison of numerical and experimental results** |
|---|---|
| Small amplitude oscillatory shear, $G'(\omega), G''(\omega)$ | Model fitted to this set of experimental data and providing accurate description of $G'$ and $G''$ over 4 decades of applied frequencies ($\omega = 0.01 - 200$ rad s$^{-1}$). |
| Shear stress relaxation after step strain, $G(t)$ | Model accurately captures stress relaxation at long times for all step strains. Beyond $\gamma_0 = 6$ the strain-softening at short times is under predicted compared to the experimental data. |
| Normal stress relaxation after step strain, $N_1(t)/\tau_{xy}(t)$ | Lodge Meissner rule followed by VCM model up to $N_1/\tau_{xy} = 2$, compared with $N_1/\tau_{xy} = 8$ for the experimental system. |
| Shear stresses in steady shearing flow, $\eta(\dot{\gamma})$ | Good agreement of $\tau_{xy}$ between model and experiments below the stress plateau. Above this, the assumption of homogeneous kinematics fails to describe the onset of the stress plateau observed experimentally. This can be captured by more detailed inhomogeneous flow calculations, see Fig .14 Zhou *et al.* (2008). |
| Normal stress differences in steady shearing flow, $N_1(\dot{\gamma}), N_2(\dot{\gamma})$ | Good agreement for $N_1$ at shear rates before onset of inhomogeneous flow; non-monotonic flow curve calculated for higher shear rates in contrast to monotonically increasing $N_1$ measured experimentally. Model unable to predict a non-zero value of $N_2$. |
| Start up of shearing flow, $\eta^+(\dot{\gamma})$ | The model closely depicts stress growth for shear rates below the onset of inhomogeneous flow. Model also capable of predicting overshoots in shear stress $\tau_{xy}$ at large step strain rates observed in experiments. |
| Cessation of steady shearing flow, $\eta^-(\dot{\gamma})$ | The rate of stress relaxation is well described at long times for all shear rates. For shear rates above the critical rate for onset of inhomogeneous flow the model does not accurately capture the stress relaxation at short times. |

Table .2. Overview comparing the results caclulated from the VCM model with those measured for the CPyCl/NaSal system.

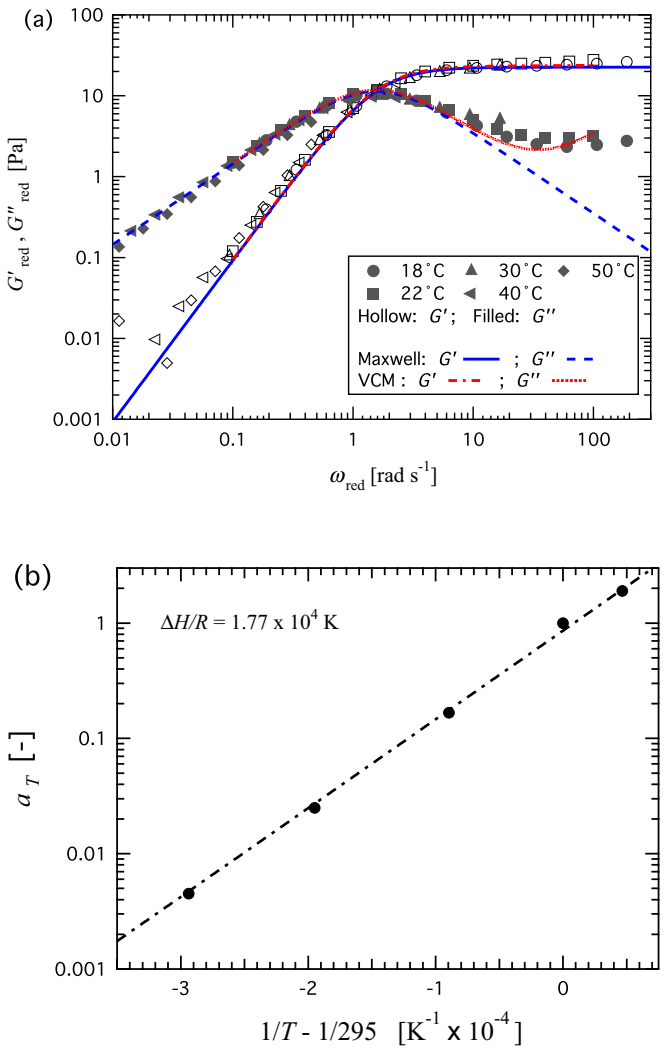


Fig. .1. (a) Reduced values of the storage (hollow) and loss (filled symbols) moduli $G'_{\mathrm{red}}$ and $G''_{\mathrm{red}}$ of the 100 mM/50 mM CpyCl/NaSal solution as a function of reduced angular frequency $\omega_{\mathrm{red}} = \omega a_T$ for temperatures in the range 18–50°C reduced with respect to $T_0 = 22$°C. (b) Evolution in the shift factor and determination of the Arrhenius activation energy $\Delta H = 1.47 \times 10^5$ J/mol for the CpyCl/NaSal solution.

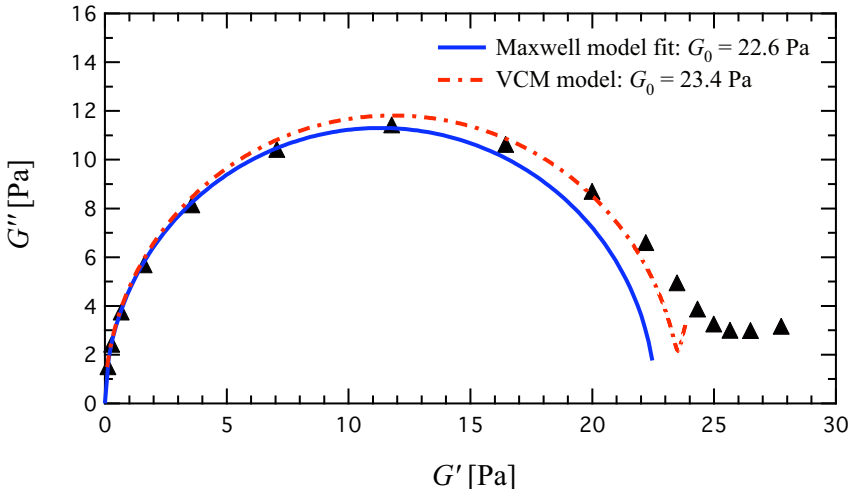


Fig. .2. Cole-Cole plot, $T = 22°$C.

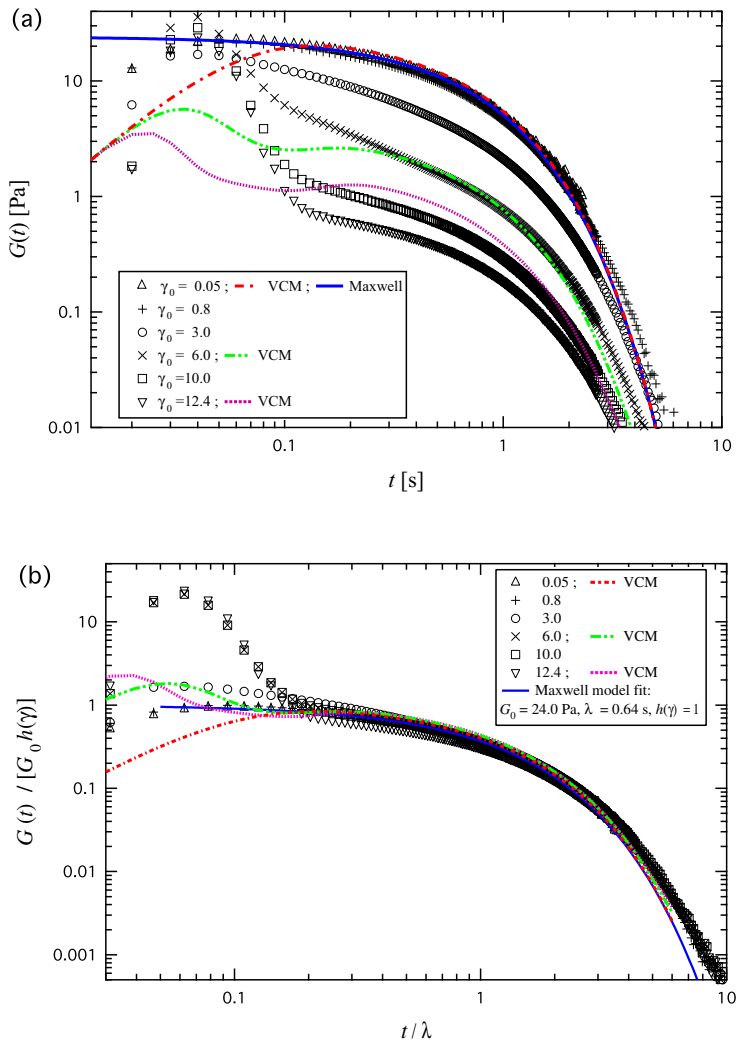


Fig. .3. Stress relaxation as a function of time after a step strain is applied at $t = 0$ s to a sample initially at rest. (a): elastic modulus $G(t) = \tau_{xy}(t, \gamma)/\gamma_0$ versus time, and (b): normalized elastic modulus $G(t)/G_{\text{eff}}$ versus time.

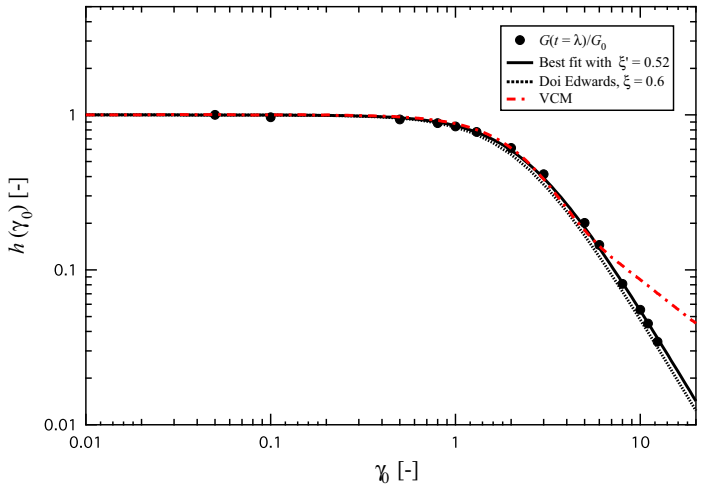


Fig. .4. Damping function $h(\gamma_0)$ as a function of the applied strain amplitude in a step strain experiment. Note that increasing the value of $c_{B\mathrm{eq}}$ will improve the prediction from the VCM model. Further refinement of the model, including variations of $c_B$ with the flow conditions, can be studied.

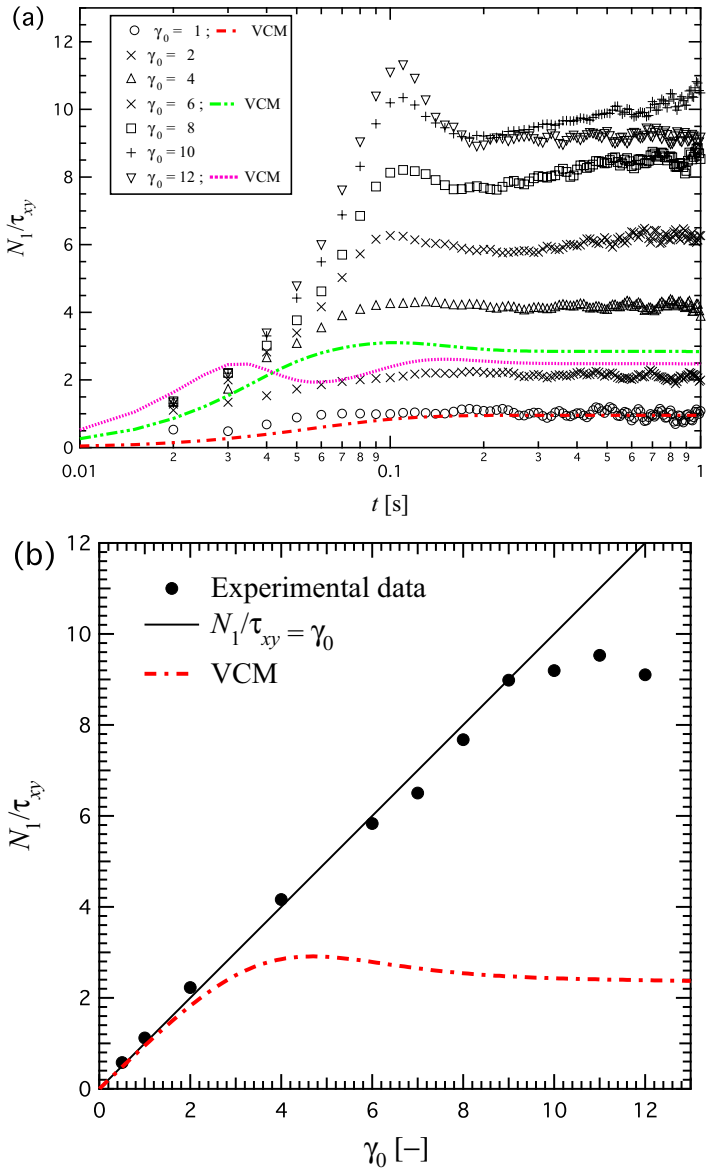


Fig. .5. After applying a step strain to the sample: (a) time evolution of the ratio of the first normal stress difference and shear stress $N_1/\tau_{xy}$ after a step strain; (b) $N_1/\tau_{xy}$ at $t = 0.2$ s as a function of applied strain.

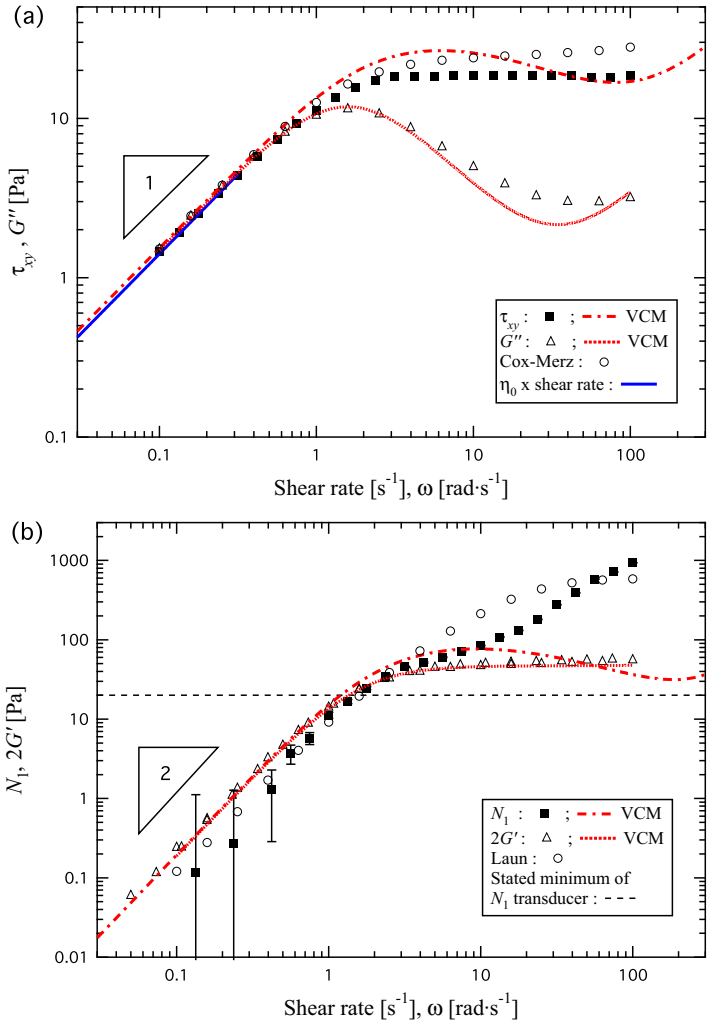


Fig. .6. Steady flow curves and comparison with viscometric properties in small amplitude oscillatory shear: top, shear stress versus shear rate, and bottom, first normal stress difference verses shear rate.

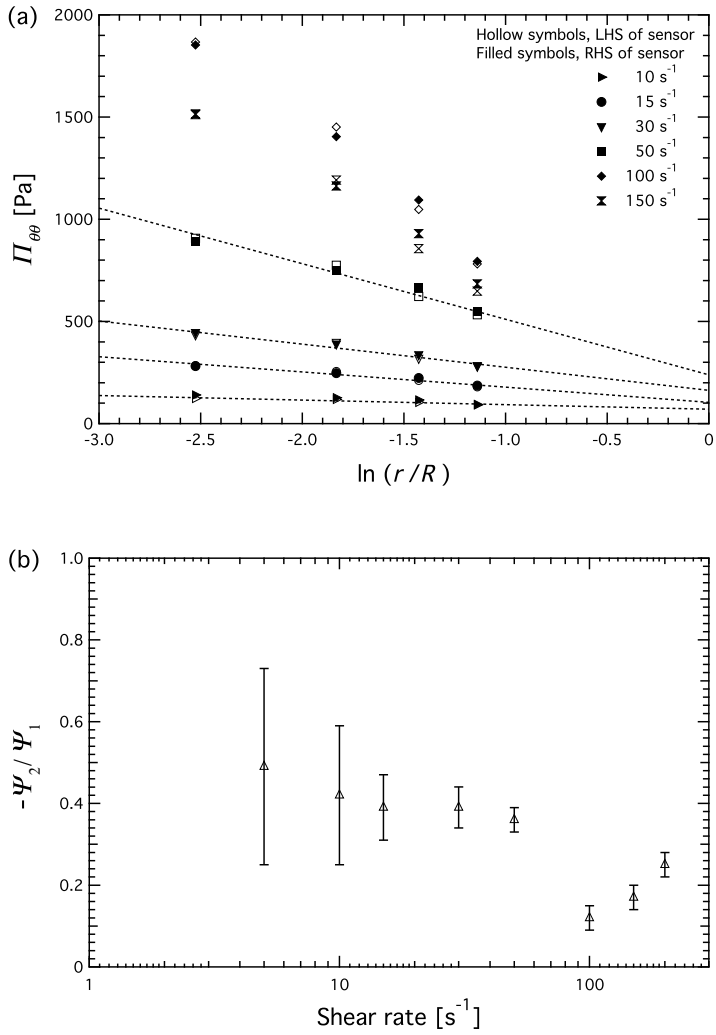


Fig. .7. (a): Total stress acting normal to the plate as a function of radius $r$ for a range of shear rates; dashed lines indicate linear fits to the data. The pressure sensing device is symmetric about the centre and data from the left hand side (hollow) and the right hand side (filled symbols) are presented. (b) Ratio of second to first normal stress coefficient $-\Psi_2/\Psi_1$ as a function of shear rate. For these data $T = 21.2 \pm 0.3^{\circ}$C.

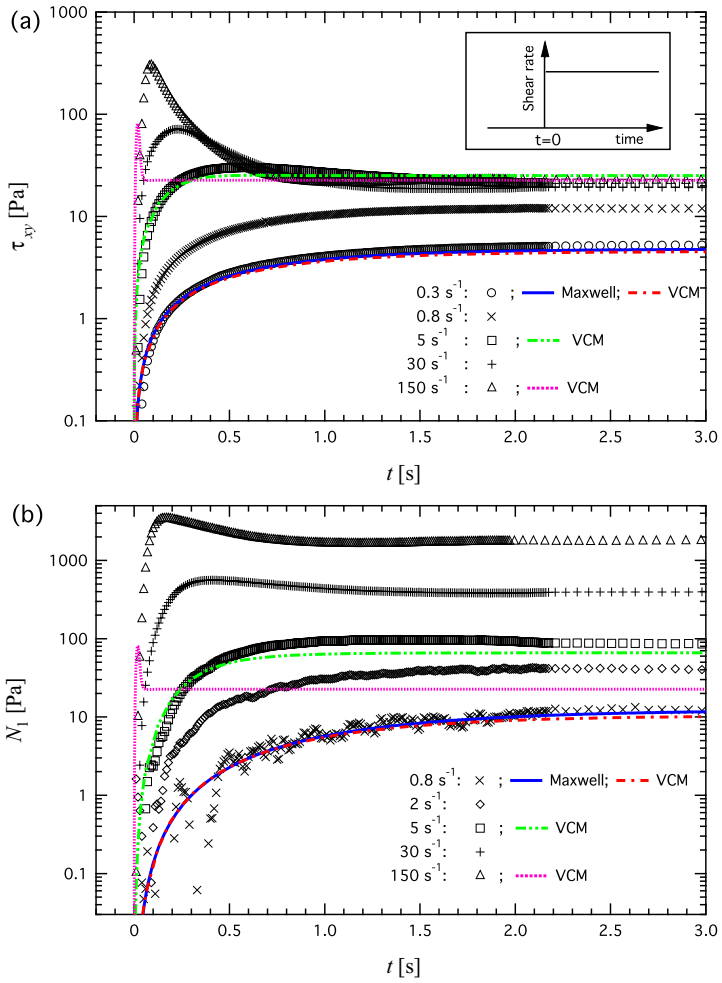


Fig. .8. Stress growth as a function of time after the inception of steady shear flow at time $t = 0$ s to a sample initially at rest. Top: shear stress $\tau_{xy}$ versus time, and bottom: first normal stress difference $N_1$ versus time.

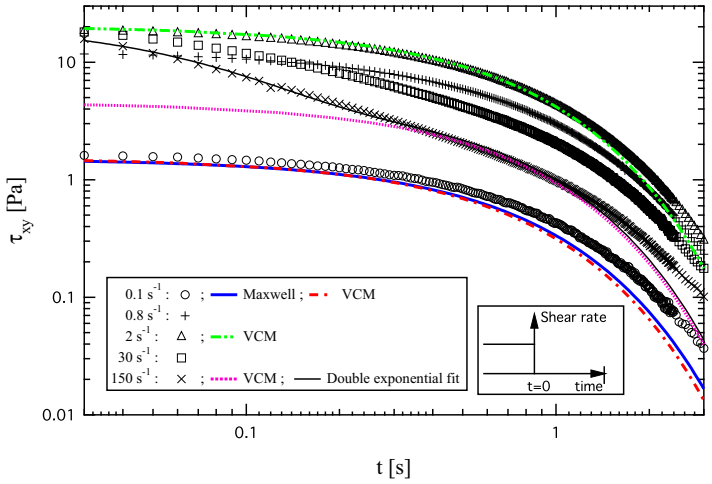


Fig. .9. Shear stress $\tau_{xy}$ versus time after a flow is turned off at $t = 0$ s.

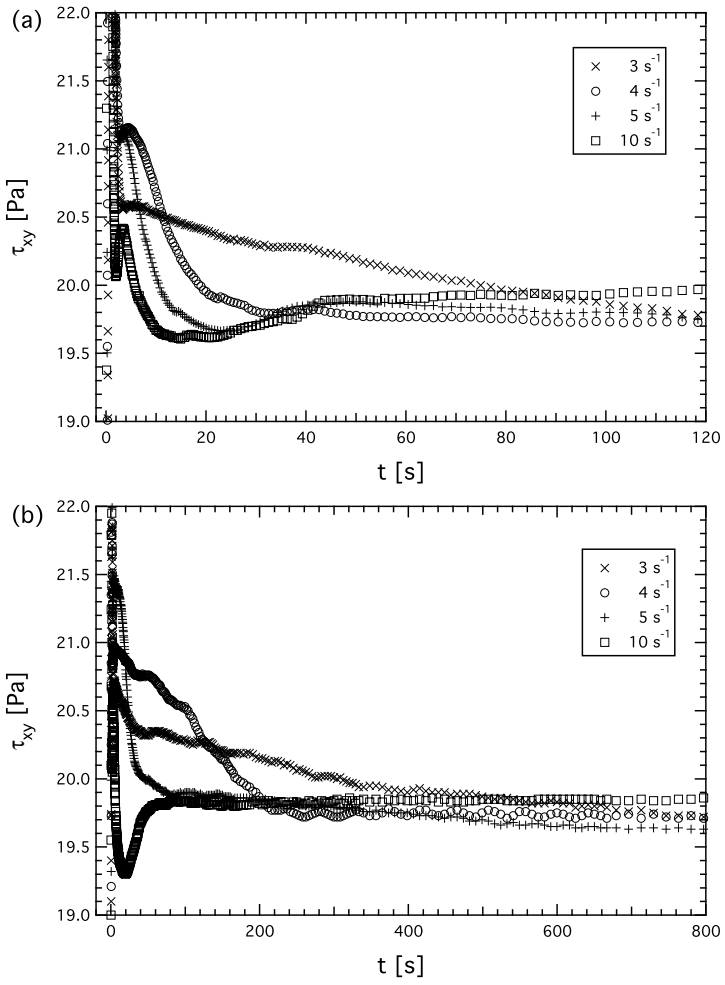


Fig. .10. Shear stress $\tau_{xy}$ versus time after a step strain rate is applied at time $t = 0$ s to a sample initially at rest. Top: experiment performed using a controlled rate rheometer (ARES), and bottom: experiment performed using a controlled stress rheometer (AR-G2).

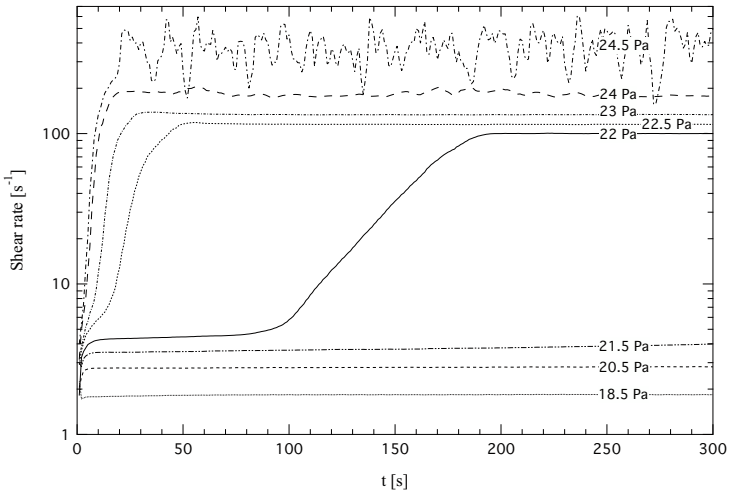


Fig. .11. Evolution in the apparent shear rate $\dot{\gamma}$ versus time after a step increase in the shear stress $\tau_{xy\ 0}$ is applied at time $t = 0$ s to a sample initially at rest.

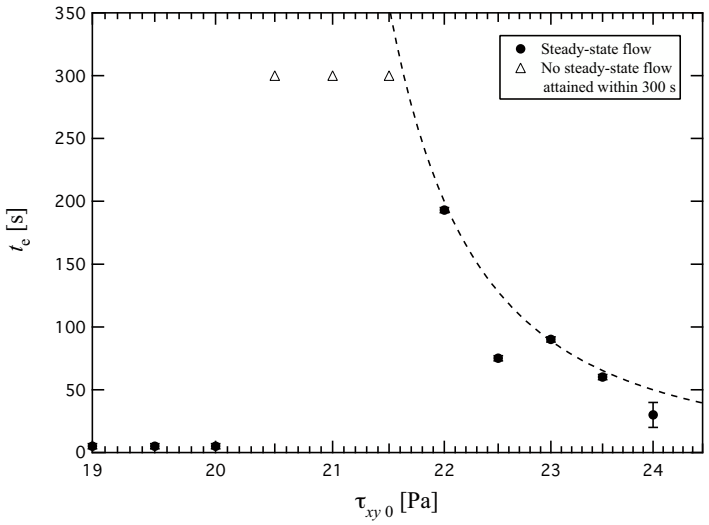


Fig. .12. Time required to reach steady state flow $t_{\rm e}$ versus applied shear stress $\tau_{xy\ 0}$ is applied at time $t = 0$ s to a sample at rest. Filled circles indicate that steady-state flow was reached; hollow triangles indicate that no steady state flow was attained after 300 s; the dashed line is an exponential decrease to guide the eye.

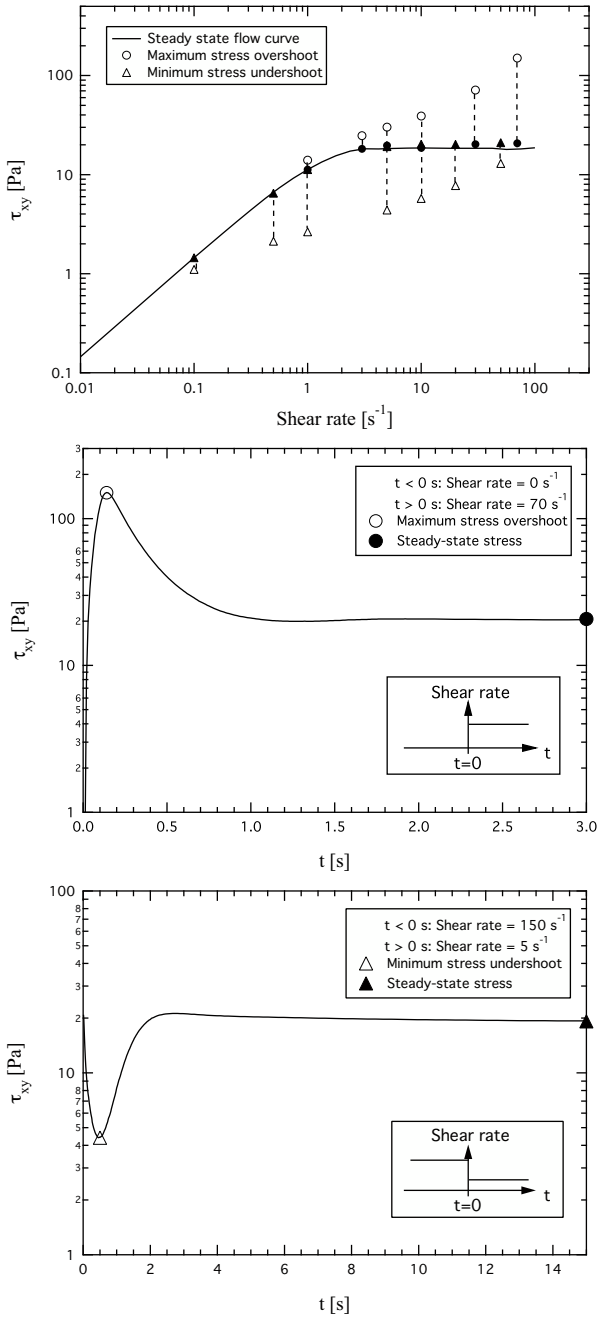


Fig. .13. Top: flow curve envelope showing maximum and minimum measured shear stress after a step in shear rate. Centre: Shear stress growth as a function of time after the inception of steady shear flow at time $t = 0$ s to a sample initially at rest. Bottom: shear stress evolution as a function of time after decreasing the steady shear rate from 150 $s^{-1}$ to 5 $s^{-1}$ at time $t = 0$ s.

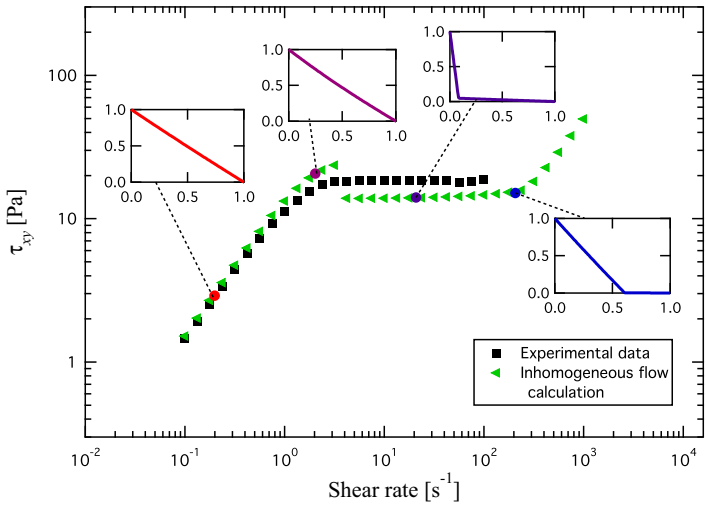


Fig. .14. Comparison of experimental steady flow curve with inhomogeneous model. The inset figures are profiles of the non-dimensional velocity (ordinate) plotted as a function of the non-dimensional radius (absicissor) computed for a narrow gap Couette cell, and correspond to the indicated points of the flow curve. Calculations of inhomogeneous VCM model courtesy of Lin Zhou. The parameters for these calculations are $\mu = 10$, $\epsilon = 10^{-4}$, $\xi = 0.45$, $c_{Aeq} = 9$, $c_{Beq} = 14.0184$, $\lambda = 0.63$ s.